

Long-lived heavy neutral leptons from mesons in effective field theory

Rebeca Beltrán,^a Giovanna Cottin,^{b,c} Juan Carlos Helo,^{d,c} Martin Hirsch,^a Arsenii Titov,^e Zeren Simon Wang^{f,g}

^a*AHEP Group, Instituto de Física Corpuscular – CSIC/Universitat de València, Apartado 22085, E-46071 València, Spain*

^b*Departamento de Ciencias, Facultad de Artes Liberales, Universidad Adolfo Ibáñez, Diagonal Las Torres 2640, Santiago, Chile*

^c*Millennium Institute for Subatomic Physics at the High Energy Frontier (SAPHIR), Fernández Concha 700, Santiago, Chile*

^d*Departamento de Física, Facultad de Ciencias, Universidad de La Serena, Avenida Cisternas 1200, La Serena, Chile*

^e*Departament de Física Teòrica, Universitat de València and Instituto de Física Corpuscular – CSIC/Universitat de València, Dr. Moliner 50, E-46100 Burjassot, Spain*

^f*Department of Physics, National Tsing Hua University, Hsinchu 300, Taiwan*

^g*Center for Theory and Computation, National Tsing Hua University, Hsinchu 300, Taiwan*

E-mail: rebeca.beltran@ific.uv.es, giovanna.cottin@uai.cl,
jchelo@userena.cl, mahirsch@ific.uv.es, arsenii.titov@ific.uv.es,
wzs@mx.nthu.edu.tw

ABSTRACT: In the framework of the low-energy effective field theory of the Standard Model extended with heavy neutral leptons (HNLs), we calculate the production rates of HNLs from meson decays triggered by dimension-six operators. We consider both lepton-number-conserving and lepton-number-violating four-fermion operators involving either a pair of HNLs or a single HNL. Assuming that HNLs are long-lived, we perform simulations and investigate the reach of the proposed far detectors at the high-luminosity LHC to (i) active-heavy neutrino mixing and (ii) the Wilson coefficients associated with the effective operators, for HNL masses below the mass of the B -meson. We further convert the latter to the associated new-physics scales. Our results show that scales in excess of hundreds of TeV and the active-heavy mixing squared as small as 10^{-15} can be probed by these experiments.

Contents

1	Introduction	1
2	Effective field theory approach	3
2.1	N_R LEFT: low-energy effective field theory with right-handed neutrinos	3
2.2	Matching to the N_R SMEFT	5
2.3	Running of the N_R LEFT operators of interest	8
2.4	An example UV completion for $d = 7$ N_R SMEFT	9
3	HNL production in meson decays	10
4	Experiments and details of simulation	15
5	Results of numerical analysis	17
6	Summary and conclusions	22
A	Pseudoscalar meson decays into HNLs	24
A.1	Two-body decays	25
A.2	Three-body decays	27
A.3	Decay constants and form factors	30
B	Branching ratios of meson decays triggered by single-N_R operators	30
C	HNL two-body decays via single-N_R operators	31

1 Introduction

The next 10–15 years will see a notable increase in experimental sensitivity to the search for heavy neutral leptons (HNLs), mostly, but not exclusively, thanks to the diverse long-lived particle program that has been initiated at CERN for the future high-luminosity LHC (HL-LHC) [1, 2]. Many new and dedicated “far-detector” proposals have been put forward in this context: ANUBIS [3], AL3X [4], CODEX-b [5], FACET [6], FASER and FASER2 [7, 8], MoEDAL-MAPP1 and MAPP2 [9, 10], and MATHUSLA [2, 11, 12]. Some of them have already been approved and even deployed. In particular, FASER and MoEDAL-MAPP1 will be taking data during recently started Run 3 of the LHC, whereas the rest of the program is envisioned for the HL phase.

Consequently, a number of papers have studied the discovery prospects of these (and other) future experiments for minimal HNLs, *i.e.* HNLs coupled to the Standard Model (SM)

only through active-heavy mixing, see Refs. [13–18]. Already in the minimal scenario one can expect up to four orders of magnitude improvement in mixing angles squared relative to existing constraints, for HNLs with masses up to roughly 5 GeV. Similarly, also the main detectors at the LHC can search for HNLs. However, ATLAS/CMS will be more sensitive at larger HNL masses, say, roughly 3–30 GeV; see *e.g.* Refs. [19–23]. Note that ATLAS [24] as well as CMS [25] have already published first results of searches for HNLs using displaced vertices.

HNLs could appear also in SM extensions with additional particles, a prominent example being a Z' . For sensitivity estimates for this scenario, see *e.g.* Refs. [26, 27]. However, since the LHC has so far not found any unambiguous signal of beyond the Standard Model (BSM) physics, attention has shifted recently towards effective field theories (EFTs). At the center-of-mass energy of the LHC, one expects that the correct description is the Standard Model effective field theory (SMEFT) (see Ref. [28] for a review) or, if we allow also for the existence of light (with masses below or around the electroweak scale) right-handed (RH) gauge singlet fermions N_R , the N_R SMEFT [29–32]. Recently, we have studied the expectation for HNL searches in the N_R SMEFT for pair- N_R operators [33] and for single- N_R operators [34].

However, below the electroweak scale, and in particular, at the scale of meson masses, the massive gauge and Higgs bosons, as well as the top quark, have to be integrated out. The correct EFT in this lower energy regime is then usually called LEFT (low-energy effective field theory) [35], or in case we add RH singlet states, N_R LEFT [36–39]. The sensitivities of future far detectors at the LHC for the four-fermion N_R LEFT operators containing a single N_R , a charged lepton ℓ , and a quark bilinear, and thus, triggering decays of mesons (produced in pp collisions at the LHC) into N_R and ℓ , have already been studied in Ref. [17]. Furthermore, the projected sensitivities of Belle II to the same set of operators have been derived in Ref. [40] (see also Ref. [41]). Therefore, in the current work, we will concentrate on pair- N_R operators and operators with one N_R and one SM neutrino, exploring the potential of future far detectors at the LHC. We note that Ref. [38] has studied a similar set of operators and derived bounds from current data on the coherent elastic neutrino-nucleus scattering (CE ν NS) process and invisible decays of light unflavored mesons.

The rest of this paper is organized as follows. In the next section, we discuss N_R LEFT operators at $d = 6$ and their matching to the N_R SMEFT at $d = 6$ and $d = 7$. Then in section 3, we elaborate on HNL production from meson decays in the framework of the N_R LEFT. Section 4 gives a brief summary of the experiments we consider and provides the corresponding simulation details. In section 5, we present the results of our simulation. We then close with a brief summary. Technical details of the computations of meson and HNL decay widths in the N_R LEFT are relegated to the appendices.

2 Effective field theory approach

2.1 N_R LEFT: low-energy effective field theory with right-handed neutrinos

In the present work, we are interested in the HNL production from meson decays in an EFT approach. Meson decays take place at energy scales $E \sim \mathcal{O}(1)$ GeV, much smaller than the electroweak scale $v = 246$ GeV. At such energies, the W and Z gauge bosons, the Higgs boson and the top quark are not propagating degrees of freedom, and the effects of potential new physics (NP) associated with a scale $\Lambda \gg E$ can be described in terms of the LEFT extended with RH neutrinos (or HNLs), N_R . We will refer to such minimal extension of the LEFT as N_R LEFT. This EFT respects $SU(3)_C \times U(1)_{\text{em}}$ gauge symmetry and in addition to the gluons and the photon contains all SM leptons, u, d, s, c, b quarks and, in general, an arbitrary number n_N of HNLs.

In addition to the renormalizable terms and higher-dimensional operators constructed from the SM fields that have been systematically classified up to $d = 6$ in Ref. [35], the N_R LEFT Lagrangian includes operators with N_R , which at $d \leq 6$ have been constructed in Refs. [37, 38]. The renormalizable part of the Lagrangian is given by

$$\mathcal{L}_{\text{ren}} = \mathcal{L}_{\text{QCD+QED}} + \overline{N_R} i \not{\partial} N_R - \left[\frac{1}{2} \overline{\nu_L} M_\nu \nu_L^c + \frac{1}{2} \overline{N_R^c} M_N N_R + \overline{\nu_L} M_D N_R + \text{h.c.} \right], \quad (2.1)$$

where $\mathcal{L}_{\text{QCD+QED}}$ is the QCD and QED Lagrangian built out of the SM leptons (including left-handed (LH) neutrinos ν_L without any mass term) and the five aforementioned flavors of quarks (for its form, see *e.g.* Eq. (5.1) in Ref. [35]). The superscript c denotes a charge conjugate field, $\psi^c \equiv C \overline{\psi}^T$. The Majorana mass matrices M_ν and M_N are complex symmetric 3×3 and $n_N \times n_N$ matrices, respectively. M_D is a generic $3 \times n_N$ Dirac mass matrix. If lepton number is conserved, the Majorana mass terms are not present. The full N_R LEFT Lagrangian reads

$$\mathcal{L}_{N_R\text{LEFT}} = \mathcal{L}_{\text{ren}} + \sum_{d \geq 5} \sum_i c_i^{(d)} \mathcal{O}_i^{(d)}, \quad (2.2)$$

where $c_i^{(d)}$ are the Wilson coefficients of higher-dimensional operators $\mathcal{O}_i^{(d)}$, and the second sum goes over all independent operators of a given mass dimension d . The dimensionful coefficients $c_i^{(d)}$ scale as Λ^{4-d} .

At $d = 5$, there are two dipole operators with N_R :

$$\mathcal{O}_{NN\gamma} = \overline{N_R^c} \sigma^{\mu\nu} N_R F_{\mu\nu} \quad \text{and} \quad \mathcal{O}_{\nu N\gamma} = \overline{\nu_L} \sigma^{\mu\nu} N_R F_{\mu\nu}, \quad (2.3)$$

where $F_{\mu\nu}$ is the photon field strength tensor. The first of these operators is antisymmetric in the HNL generation indices, and thus, it vanishes identically for $n_N = 1$. $\mathcal{O}_{NN\gamma}$ is lepton-number-violating (LNV), whereas $\mathcal{O}_{\nu N\gamma}$ is lepton-number-conserving (LNC). The phenomenology of the RH neutrino dipole operator has been studied in Ref. [30] and more recently in Ref. [42] in the context of the proposed far detectors at the LHC.

	Name	Structure	$n_N = 1$	$n_N = 3$
LNC	$\mathcal{O}_{dN}^{V,RR}$	$(\bar{d}_R \gamma_\mu d_R) (\bar{N}_R \gamma^\mu N_R)$	9	81
	$\mathcal{O}_{uN}^{V,RR}$	$(\bar{u}_R \gamma_\mu u_R) (\bar{N}_R \gamma^\mu N_R)$	4	36
	$\mathcal{O}_{dN}^{V,LR}$	$(\bar{d}_L \gamma_\mu d_L) (\bar{N}_R \gamma^\mu N_R)$	9	81
	$\mathcal{O}_{uN}^{V,LR}$	$(\bar{u}_L \gamma_\mu u_L) (\bar{N}_R \gamma^\mu N_R)$	4	36
LNV	$\mathcal{O}_{dN}^{S,RR}$	$(\bar{d}_L d_R) (\bar{N}_R^c N_R)$	18	108
	$\mathcal{O}_{dN}^{T,RR}$	$(\bar{d}_L \sigma_{\mu\nu} d_R) (\bar{N}_R^c \sigma^{\mu\nu} N_R)$	0	54
	$\mathcal{O}_{uN}^{S,RR}$	$(\bar{u}_L u_R) (\bar{N}_R^c N_R)$	8	48
	$\mathcal{O}_{uN}^{T,RR}$	$(\bar{u}_L \sigma_{\mu\nu} u_R) (\bar{N}_R^c \sigma^{\mu\nu} N_R)$	0	24
	$\mathcal{O}_{dN}^{S,LR}$	$(\bar{d}_R d_L) (\bar{N}_R^c N_R)$	18	108
	$\mathcal{O}_{uN}^{S,LR}$	$(\bar{u}_R u_L) (\bar{N}_R^c N_R)$	8	48

Table 1. Dimension-six operators in the N_R LEFT, involving two quarks and two HNLs. For each operator structure, we give the number of independent real parameters for $n_N = 1$ and $n_N = 3$ generations of N_R . We recall that in the N_R LEFT, $n_d = 3$ and $n_u = 2$. The LNV operator structures require “+h.c.”.

At $d = 6$, there are 55 four-fermion interactions, of which 23 LNC [37], 26 LNV, and six operators that violate both lepton and baryon numbers [38].¹ The contact operators triggering meson decays into HNLs involve a pair of quarks and a leptonic part, which in turn contains either (i) a pair of HNLs, or (ii) N_R and ν_L , or else (iii) N_R and a charged lepton. The last possibility has been investigated in detail in Refs. [17] and [40], in the context of long-lived HNLs that could be produced in meson decays at the high-luminosity LHC and Belle II, respectively. In this work, we focus on the operators with neutral leptons. In tables 1 and 2, we summarize the pair- N_R and single- N_R operators of interest. Though in our numerical analysis we will focus on the case of a single HNL generation ($n_N = 1$), in the tables we provide for completeness the numbers of independent real parameters associated with each operator for $n_N = 1$ and $n_N = 3$. We have checked these numbers using the `Sym2Int` package [43, 44]. In the group of pair- N_R operators, there are four LNC structures and six LNV ones (of which two vanish identically for $n_N = 1$). Among the single- N_R operators, six structures conserve lepton number, whereas four violate it.

¹Here, we do not count possible flavor structures and Hermitian conjugates.

	Name	Structure	$n_N = 1$	$n_N = 3$
LNC	$\mathcal{O}_{d\nu N}^{S,RR}$	$(\bar{d}_L d_R) (\bar{\nu}_L N_R)$	54	162
	$\mathcal{O}_{d\nu N}^{T,RR}$	$(\bar{d}_L \sigma_{\mu\nu} d_R) (\bar{\nu}_L \sigma^{\mu\nu} N_R)$	54	162
	$\mathcal{O}_{u\nu N}^{S,RR}$	$(\bar{u}_L u_R) (\bar{\nu}_L N_R)$	24	72
	$\mathcal{O}_{u\nu N}^{T,RR}$	$(\bar{u}_L \sigma_{\mu\nu} u_R) (\bar{\nu}_L \sigma^{\mu\nu} N_R)$	24	72
	$\mathcal{O}_{d\nu N}^{S,LR}$	$(\bar{d}_R d_L) (\bar{\nu}_L N_R)$	54	162
	$\mathcal{O}_{u\nu N}^{S,LR}$	$(\bar{u}_R u_L) (\bar{\nu}_L N_R)$	24	72
LNV	$\mathcal{O}_{d\nu N}^{V,RR}$	$(\bar{d}_R \gamma_\mu d_R) (\bar{\nu}_L^c \gamma^\mu N_R)$	54	162
	$\mathcal{O}_{u\nu N}^{V,RR}$	$(\bar{u}_R \gamma_\mu u_R) (\bar{\nu}_L^c \gamma^\mu N_R)$	24	72
	$\mathcal{O}_{d\nu N}^{V,LR}$	$(\bar{d}_L \gamma_\mu d_L) (\bar{\nu}_L^c \gamma^\mu N_R)$	54	162
	$\mathcal{O}_{u\nu N}^{V,LR}$	$(\bar{u}_L \gamma_\mu u_L) (\bar{\nu}_L^c \gamma^\mu N_R)$	24	72

Table 2. Dimension-six operators in the N_R LEFT, involving two quarks, one active neutrino and one HNL. For each operator structure, we give the number of independent real parameters for $n_N = 1$ and $n_N = 3$ generations of N_R . We recall that in the N_R LEFT, $n_\nu = n_d = 3$ and $n_u = 2$. All operator structures require “+h.c.”.

2.2 Matching to the N_R SMEFT

In this subsection, we assume that the N_R LEFT originates from the N_R SMEFT,² *i.e.* the EFT of the SM extended with RH neutrinos [29–31]. The N_R SMEFT respects the SM gauge symmetry $SU(3)_C \times SU(2)_L \times U(1)_Y$, and it is valid at energies above the electroweak scale, set by the vacuum expectation value (VEV) of the Higgs, v . In the considered case of the N_R LEFT as the low-energy limit of the N_R SMEFT, there are no new particles at energies between E and v , and the N_R LEFT scale Λ can be identified with v . At this scale, the two EFTs must be matched.

At tree level, the matching of the $d = 6$ LNC operators has been worked out in Ref. [37] and that of the $d = 6$ LNV operators in Ref. [38].³ Below we summarize the results of this matching relevant to the operators of interest. The N_R SMEFT operators contributing to the matching relations for the coefficients of the N_R LEFT operators from tables 1 and 2 are given in tables 3 and 4, respectively. For the dimensionful Wilson coefficients of the N_R SMEFT operators, we use capital $C_i^{(d)}$. They scale as $\Lambda_{\text{NP}}^{4-d}$, where $\Lambda_{\text{NP}} \gg v$ is the scale of new physics. For simplicity, we assume only one generation of N_R , while considering

²It is worth noting that (N_R) LEFT is the correct effective description at low energies even if the high-energy EFT is not given by the (N_R) SMEFT but by the HEFT (with N_R), in which the Higgs is not part of a fundamental weak doublet [35].

³For the N_R LEFT operators with two quarks, a charged lepton and a neutrino, the tree-level matching has been performed also in Refs. [17, 45]. For the first-generation charged fermions, such operators contribute, among other processes, to neutrinoless double beta decay [45–48].

	Name	Structure	$n_N = 1$	$n_N = 3$
$d = 6$ (LNC)	\mathcal{O}_{dN}	$(\bar{d}_R \gamma_\mu d_R) (\bar{N}_R \gamma^\mu N_R)$	9	81
	\mathcal{O}_{uN}	$(\bar{u}_R \gamma_\mu u_R) (\bar{N}_R \gamma^\mu N_R)$	9	81
	\mathcal{O}_{QN}	$(\bar{Q} \gamma_\mu Q) (\bar{N}_R \gamma^\mu N_R)$	9	81
	\mathcal{O}_{HN}	$(H^\dagger i \overleftrightarrow{D}_\mu H) (\bar{N}_R \gamma^\mu N_R)$	1	9
$d = 7$ (LNV)	\mathcal{O}_{QNdH}	$(\bar{Q} N_R) (\bar{N}_R^c d_R) H$	18	162
	\mathcal{O}_{dQNH}	$H^\dagger (\bar{d}_R Q) (\bar{N}_R^c N_R)$	18	108
	\mathcal{O}_{QNuH}	$(\bar{Q} N_R) (\bar{N}_R^c u_R) \tilde{H}$	18	162
	\mathcal{O}_{uQNH}	$\tilde{H}^\dagger (\bar{u}_R Q) (\bar{N}_R^c N_R)$	18	108

Table 3. Dimension-six and dimension-seven operators in the N_R SMEFT contributing to the tree-level matching relations for the Wilson coefficients of the dimension-six N_R LEFT operators from table 1. For each operator structure, we give the number of independent real parameters for $n_N = 1$ and $n_N = 3$ generations of N_R . The LNV operator structures require “+h.c.”.

	Name	Structure	$n_N = 1$	$n_N = 3$
$d = 6$ (LNC)	\mathcal{O}_{LNQd}	$\epsilon_{ab} (\bar{L}^a N_R) (\bar{Q}^b d_R)$	54	162
	\mathcal{O}_{LdQN}	$\epsilon_{ab} (\bar{L}^a d_R) (\bar{Q}^b N_R)$	54	162
	\mathcal{O}_{QuNL}	$(\bar{Q} u_R) (\bar{N}_R L)$	54	162
$d = 7$ (LNV)	\mathcal{O}_{dNLH}	$\epsilon_{ab} (\bar{d}_R \gamma_\mu d_R) (\bar{N}_R^c \gamma^\mu L^a) H^b$	54	162
	\mathcal{O}_{uNLH}	$\epsilon_{ab} (\bar{u}_R \gamma_\mu u_R) (\bar{N}_R^c \gamma^\mu L^a) H^b$	54	162
	\mathcal{O}_{QNLH1}	$\epsilon_{ab} (\bar{Q} \gamma_\mu Q) (\bar{N}_R^c \gamma^\mu L^a) H^b$	54	162
	\mathcal{O}_{QNLH2}	$\epsilon_{ab} (\bar{Q} \gamma_\mu Q^a) (\bar{N}_R^c \gamma^\mu L^b) H$	54	162
	\mathcal{O}_{NL1}	$\epsilon_{ab} (\bar{N}_R^c \gamma_\mu L^a) (i D^\mu H^b) (H^\dagger H)$	6	18
	\mathcal{O}_{NL2}	$\epsilon_{ab} (\bar{N}_R^c \gamma_\mu L^a) H^b (H^\dagger i \overleftrightarrow{D}^\mu H)$	6	18

Table 4. Dimension-six and dimension-seven operators in the N_R SMEFT contributing to the tree-level matching relations for the Wilson coefficients of the dimension-six N_R LEFT operators from table 2. For each operator structure, we give the number of independent real parameters for $n_N = 1$ and $n_N = 3$ generations of N_R . All operator structures require “+h.c.”.

a general structure of quark, charged lepton and LH neutrino flavor indices. We denote the quark flavor indices by i, j and the lepton flavor index by α . Furthermore, we assume that in the N_R LEFT, quarks are in the mass basis, whereas the N_R SMEFT operators are written in the weak interaction basis.

The matching conditions for the coefficients of the LNC pair- N_R operators holding at

the electroweak scale read:

$$c_{dN,ij}^{V,RR} = C_{dN}^{ij} - \frac{g_Z^2}{m_Z^2} Z_{dR}^{ij} Z_N, \quad c_{uN,ij}^{V,RR} = C_{uN}^{ij} - \frac{g_Z^2}{m_Z^2} Z_{uR}^{ij} Z_N, \quad (2.4)$$

$$c_{dN,ij}^{V,LR} = V_{ki}^* V_{lj} C_{QN}^{kl} - \frac{g_Z^2}{m_Z^2} Z_{dL}^{ij} Z_N, \quad c_{uN,ij}^{V,LR} = C_{QN}^{ij} - \frac{g_Z^2}{m_Z^2} Z_{uL}^{ij} Z_N. \quad (2.5)$$

Here, V is the CKM matrix defined through $d'_L = V d_L$, where d' and d are flavor and mass eigenstates, respectively. In addition,

$$g_Z \equiv \frac{e}{s_W c_W}, \quad Z_\psi^{ij} \equiv (T_\psi^3 - Q_\psi s_W^2) \delta^{ij}, \quad Z_N \equiv -\frac{v^2}{2} C_{HN}, \quad (2.6)$$

with ψ denoting a SM fermion, and T_ψ^3 and Q_ψ being its weak isospin and electric charge, respectively. Further, $s_W \equiv \sin \theta_W$ and $c_W \equiv \cos \theta_W$, where θ_W is the weak mixing angle, and m_Z is the mass of the Z boson. Note that in Z_ψ^{ij} we neglect the contributions of $d = 6$ N_R SMEFT operators (cf. Eq. (2.18) in Ref. [38]), since when multiplied by Z_N these would lead to $d = 8$ effects.

For the LNC single- N_R operators, we have:

$$c_{d\nu N,ij\alpha}^{S,RR} = V_{ki}^* \left(C_{LNQd}^{\alpha kj} - \frac{1}{2} C_{LdQN}^{\alpha jk} \right), \quad c_{d\nu N,ij\alpha}^{T,RR} = -\frac{1}{8} V_{ki}^* C_{LdQN}^{\alpha jk}, \quad (2.7)$$

$$c_{u\nu N,ij\alpha}^{S,RR} = 0, \quad c_{u\nu N,ij\alpha}^{T,RR} = 0, \quad (2.8)$$

$$c_{d\nu N,ij\alpha}^{S,LR} = 0, \quad c_{u\nu N,ij\alpha}^{S,LR} = C_{QuNL}^{ji\alpha*}. \quad (2.9)$$

We note that the Higgs exchange contributions (which a priori seem relevant) are parametrically of the same order as $d = 8$ terms, and thus, can be dropped when working to $d = 6$ [35].

In the N_R SMEFT at $d = 6$, there is only one operator which violates lepton number, but conserves baryon number, namely, $\mathcal{O}_{NNNN} = (\bar{N}_R^c N_R)(\bar{N}_R^c N_R)$. It vanishes identically in the case of one generation of N_R . Thus, the $d = 6$ LNV operators in the N_R LEFT are expected to get contributions from $d = 7$ LNV operators in the N_R SMEFT. A basis of the latter can be found in Ref. [31] (see also Ref. [49]). A subset of the $d = 7$ operators relevant for the matching we are interested in is collected in the bottom part of tables 3 and 4.

For the LNV pair- N_R operators, the matching conditions read:

$$c_{dN,ij}^{S,RR} = -\frac{v}{2\sqrt{2}} V_{ki}^* C_{QN dH}^{kj}, \quad c_{uN,ij}^{S,RR} = -\frac{v}{2\sqrt{2}} C_{QN uH}^{ij}, \quad (2.10)$$

$$c_{dN,ij}^{S,LR} = \frac{v}{\sqrt{2}} V_{kj} C_{dQH}^{ik}, \quad c_{uN,ij}^{S,LR} = \frac{v}{\sqrt{2}} C_{uQH}^{ij}. \quad (2.11)$$

Finally, for the LNV single- N_R operators, we have:

$$c_{d\nu N,ij\alpha}^{V,RR} = -\frac{v}{\sqrt{2}} C_{dNLH}^{ij\alpha} - \frac{g_Z^2}{m_Z^2} Z_{dR}^{ij} Z_{\nu N}^\alpha, \quad (2.12)$$

$$c_{u\nu N,ij\alpha}^{V,RR} = -\frac{v}{\sqrt{2}} C_{uNLH}^{ij\alpha} - \frac{g_Z^2}{m_Z^2} Z_{uR}^{ij} Z_{\nu N}^\alpha, \quad (2.13)$$

$$c_{d\nu N,ij\alpha}^{V,LR} = -\frac{v}{\sqrt{2}}V_{ki}^*V_{lj}\left(C_{QNLH1}^{kl\alpha} - C_{QNLH2}^{kl\alpha}\right) - \frac{g_Z^2}{m_Z^2}Z_{dL}^{ij}Z_{\nu N}^\alpha, \quad (2.14)$$

$$c_{u\nu N,ij\alpha}^{V,LR} = -\frac{v}{\sqrt{2}}C_{QNLH1}^{ij\alpha} - \frac{g_Z^2}{m_Z^2}Z_{uL}^{ij}Z_{\nu N}^\alpha. \quad (2.15)$$

Here, the couplings $Z_{\nu N}^\alpha$ are defined as

$$Z_{\nu N}^\alpha \equiv \frac{v^3}{4\sqrt{2}}(C_{NL1}^\alpha + 2C_{NL2}^\alpha). \quad (2.16)$$

2.3 Running of the N_R LEFT operators of interest

Between the energy scale at which meson decays take place and the weak scale, the Wilson coefficients of the N_R LEFT operators evolve according to renormalization group equations (RGEs). These are analogous to the RGEs in the LEFT (without N_R) [50], and some partial results for the operators with N_R can be found in Refs. [17, 37, 38]. Below we provide the one-loop RGEs for the pair- N_R and single- N_R operators summarized in tables 1 and 2. The operators given by the product of vector currents are renormalized by QED corrections.⁴

$$\dot{c}_{qN,ij}^{V,RR} = \dot{c}_{qN,ij}^{V,LR} = \frac{4}{3}e^2Q_qN_c\delta_{ij}\left[Q_u\left(c_{uN,kk}^{V,RR} + c_{uN,kk}^{V,LR}\right) + Q_d\left(c_{dN,kk}^{V,RR} + c_{dN,kk}^{V,LR}\right)\right], \quad (2.17)$$

$$\dot{c}_{q\nu N,ij\alpha}^{V,RR} = \dot{c}_{q\nu N,ij\alpha}^{V,LR} = \frac{4}{3}e^2Q_qN_c\delta_{ij}\left[Q_u\left(c_{u\nu N,kk\alpha}^{V,RR} + c_{u\nu N,kk\alpha}^{V,LR}\right) + Q_d\left(c_{d\nu N,kk\alpha}^{V,RR} + c_{d\nu N,kk\alpha}^{V,LR}\right)\right]. \quad (2.18)$$

Here, $\dot{c} \equiv 16\pi^2\mu\frac{dc}{d\mu}$, with μ being the renormalization scale; $q = d$ or u ; e is the QED coupling constant, Q_q is the electric charge of the quark q ; and $N_c = 3$ is the number of colors. The flavor index k runs over u and c for the up-type quarks, and over d, s, b for the down-type quarks. We see that only the coefficients with $i = j$ run, whereas those with $i \neq j$, which will be of interest to us in what follows, do not.

The operators of the scalar and tensor types are renormalized due to both QCD and QED corrections:

$$\dot{c}_q^S = -6(g^2C_F + e^2Q_q^2)c_q^S, \quad c_q^S = c_{qN,ij}^{S,RR}, c_{qN,ij}^{S,LR}, c_{q\nu N,ij\alpha}^{S,RR}, c_{q\nu N,ij\alpha}^{S,LR}, \quad (2.19)$$

$$\dot{c}_q^T = 2(g^2C_F + e^2Q_q^2)c_q^T, \quad c_q^T = c_{qN,ij}^{T,RR}, c_{q\nu N,ij\alpha}^{T,RR}, \quad (2.20)$$

where g is the strong coupling constant, and $C_F = (N_c^2 - 1)/(2N_c) = 4/3$.

Solving these RGEs to the leading-logarithm approximation, we find:

$$c_q^S(\mu) = \left[\frac{g(\mu)}{g(\mu_1)}\right]^{\frac{6C_F}{b_g}} \left[\frac{e(\mu)}{e(\mu_1)}\right]^{\frac{6Q_q^2}{b_e}} c_q^S(\mu_1), \quad (2.21)$$

$$c_q^T(\mu) = \left[\frac{g(\mu)}{g(\mu_1)}\right]^{-\frac{2C_F}{b_g}} \left[\frac{e(\mu)}{e(\mu_1)}\right]^{-\frac{2Q_q^2}{b_e}} c_q^T(\mu_1), \quad (2.22)$$

⁴In these equations, we ignore the contributions from the four-fermion leptonic operators $\mathcal{O}_{eN}^{V,RR}$ and $\mathcal{O}_{eN}^{V,LR}$ as well as from the double insertions of the $d = 5$ neutrino dipole operators.

where $\mu_1 < \mu$ are two energy scales, and b_g and b_e are the coefficients of the one-loop QCD and QED beta functions, respectively:⁵

$$b_g = \frac{11}{3}N_c - \frac{2}{3}(n_u + n_d), \quad (2.23)$$

$$b_e = -\frac{4}{3}(Q_e^2 n_e + Q_d^2 N_c n_d + Q_u^2 N_c n_u). \quad (2.24)$$

Setting $\mu_1 = m_b$ and $\mu = v$, we find

$$c_u^S(v) = 0.68 c_u^S(m_b), \quad c_d^S(v) = 0.69 c_d^S(m_b), \quad (2.25)$$

$$c_u^T(v) = 1.14 c_u^T(m_b), \quad c_d^T(v) = 1.13 c_d^T(m_b). \quad (2.26)$$

Thus, when running from m_b to v , the scalar type operators get suppressed, whereas the tensor type operator get enhanced, cf. Ref. [38]. Finally, we note that the contribution to the running from QED corrections is practically negligible.

Concerning the running in the N_R SMEFT, *i.e.* between the EW scale and the scale of new physics, Λ_{NP} , the one-loop RGEs for $d = 6$ operators with N_R have been derived in Refs. [51–53], while partial results for some $d = 7$ N_R -operators (relevant for neutrinoless double beta decay) have been obtained in Ref. [45].

2.4 An example UV completion for $d = 7$ N_R SMEFT

The operators including one or two N_R in the N_R SMEFT can be generated in the ultra-violet (UV) in a variety of ways. For example, Ref. [36] discusses all possible leptoquark states that can induce $d = 6$ N_R SMEFT operators. Also Refs. [33] and [34] study some example models for pair- N_R and single- N_R operators at $d = 6$, respectively, including leptoquark and Z' models. However, neither of these references gives example models for the $d = 7$ N_R SMEFT operators, to which our low-energy LNV N_R operators must be matched.

Here, we do not attempt to give a systematic list of such models for the $d = 7$ operators. Instead, we will briefly discuss one concrete, but very typical UV model as an example. This example model generates the operator $\mathcal{O}_{QN dH}$. For the other $d = 7$ operators containing one or two N_R , other UV models can be constructed in an analogous manner.

Our example model contains two scalar leptoquark states, $S_1 \sim (\mathbf{3}, \mathbf{1})_{-1/3}$ and $S_2 \sim (\mathbf{3}, \mathbf{2})_{1/6}$, with the numbers inside parentheses denoting the $(SU(3)_C, SU(2)_L)$ representations and the subscript standing for the hypercharge. Apart from the mass and kinetic terms for the leptoquark states, the model allows to write down the following interactions, in addition to the SM Lagrangian:

$$\mathcal{L} \supset - \left[Y_{QN} \bar{Q} N_R S_2 + Y_{Nd} \bar{N}_R^c d_R S_1^\dagger + \mu H S_2^\dagger S_1 + \text{h.c.} \right] + \cdots, \quad (2.27)$$

where, for simplicity, we have suppressed generation indices. Note that this Lagrangian violates lepton number, but lepton number is recovered in the limit $\mu \rightarrow 0$ [54]. Integrating

⁵For the beta functions, we use $\dot{g} = -b_g g^3$ and $\dot{e} = -b_e e^3$.

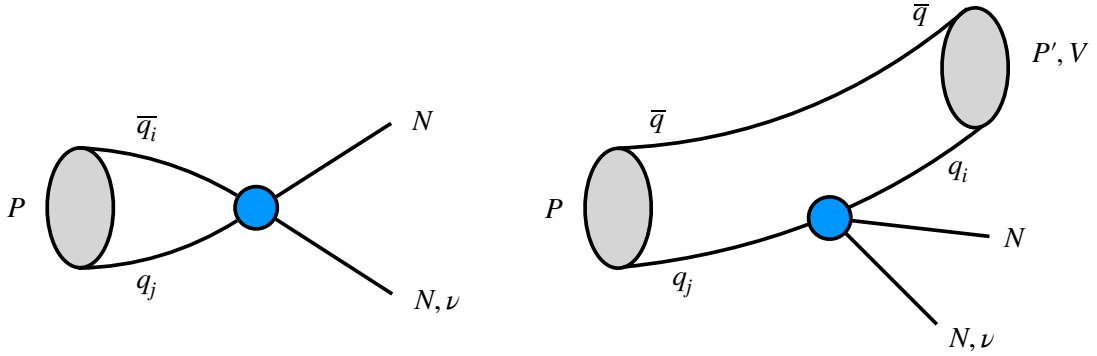


Figure 1. Two- and three-body pseudoscalar meson decays triggered by the effective operators with a pair of HNLs, or one HNL and one SM neutrino. The blue blob denotes the insertion of an effective operator. In the right diagram, the quark q can be u, d, s, c or b , whereas the quarks q_i and q_j are both of either the up- or down-type, with $m_{q_j} > m_{q_i}$. $P^{(\prime)}$ and V denote pseudoscalar and vector mesons, respectively.

out both leptoquarks will produce \mathcal{O}_{QNdH} with $C_{QNdH} = (\mu Y_{QN} Y_{Nd}) / (m_{S_1}^2 m_{S_2}^2)$. In the limit $\mu = m_{S_1} = m_{S_2} = \Lambda_{\text{NP}}$, this gives the correct $C_{QNdH} \propto \Lambda_{\text{NP}}^{-3}$ dependence for a $d = 7$ operator, as expected. Clearly, this model will also generate $d = 6$ operators with N_R . For example, the term proportional to Y_{QN} (Y_{Nd}) times its hermitian conjugate will generate \mathcal{O}_{QN} (\mathcal{O}_{dN}). However, these are only examples, as actually more $d = 6$ operators can be generated in this model; note the dots in Eq. (2.27).

3 HNL production in meson decays

We are interested in HNLs produced in meson decays. In the framework of the $N_R\text{LEFT}$, such decays are triggered by both active-heavy neutrino mixing and higher-dimensional operators. The HNL production via mixing has been studied in detail in the literature, see *e.g.* Refs. [55–57] for recent reappraisals. The HNL production via effective interactions has been considered in Ref. [17] for the four-fermion operators with two quarks, one charged lepton and N_R . In this section, we focus on the meson decay modes triggered by the operators with two quarks and two neutral leptons (either a pair of N_R , or N_R and ν_L) discussed in section 2.

Given their large production rates at the LHC, we focus on pseudoscalar mesons containing either a c or b quark and a light quark, *i.e.* D - and B -mesons. Vector mesons with the same quark content have much smaller lifetimes, and thus, their contribution in the HNL production is sub-dominant [17].

In figure 1, we depict two- and three-body pseudoscalar meson decays triggered by the effective operators of interest. The same $N_R\text{LEFT}$ operator induces a leptonic two-body decay as well as contributes to a number of semi-leptonic three-body decays. In the diagram corresponding to the three-body decay, q can be any quark but top, since the latter does not form bound states and is not present in the spectrum of the $N_R\text{LEFT}$. For

the transition $q_j \rightarrow q_i$ with $i \neq j$, both quarks have to be of either the up- or down-type, since the operators considered involve quark bilinears with zero electric charge. In addition, $m_{q_j} > m_{q_i}$ for the decay to be kinematically allowed.⁶ These considerations lead to the following four possibilities: $c \rightarrow u$ (for the up-quark sector), and $b \rightarrow d$, $b \rightarrow s$ and $s \rightarrow d$ (for the down-quark sector). Below we discuss each of them in detail.

- The operators with $q_j = c$ and $q_i = u$ lead to the leptonic two-body decays $D^0 \rightarrow NN$ and $D^0 \rightarrow \nu N$.⁷ In addition, they generate the following transitions resulting in semi-leptonic three-body decays: $D^0 \rightarrow \pi^0, \eta, \eta' (\rho^0, \omega)$ for $q = u$; $D^+ \rightarrow \pi^+ (\rho^+)$ for $q = d$; $D_s^+ \rightarrow K^+ (K^{*+})$ for $q = s$; $\eta_c \rightarrow \overline{D^0} (\overline{D^{*0}})$ for $q = c$; and $B_c^+ \rightarrow B^+ (B^{*+})$ for $q = b$. Here, the final states outside (inside) parentheses are pseudoscalar (vector) mesons. In what follows, we will not take into account the decays of η_c and B_c^+ . The η_c meson has a lifetime of $\mathcal{O}(10^{-23})$ s [58], which is much smaller than that of other pseudoscalar mesons and comparable with the lifetimes of vector mesons. Concerning B_c^+ , its production rate at the LHC is much smaller than that of D - and B -mesons, see *e.g.* Ref. [59].
- The operators with $q_j = b$ and $q_i = d$ ⁸ induce $B^0 \rightarrow NN$ and $B^0 \rightarrow \nu N$ decays, as well as the following transitions: $B^+ \rightarrow \pi^+ (\rho^+)$ for $q = u$; $B^0 \rightarrow \pi^0, \eta, \eta' (\rho^0, \omega)$ for $q = d$; $B_s^0 \rightarrow \overline{K^0} (\overline{K^{*0}})$ for $q = s$; $B_c^+ \rightarrow D^+ (D^{*+})$ for $q = c$; and $\eta_b \rightarrow \overline{B^0} (\overline{B^{*0}})$ for $q = b$. Again, we will not consider the decays of B_c^+ as well as those of η_b .
- The operators with $q_j = b$ and $q_i = s$ give rise to $B_s^0 \rightarrow NN$ and $B_s^0 \rightarrow \nu N$ decays. They also contribute to $B^+ \rightarrow K^+ (K^{*+})$ for $q = u$; $B^0 \rightarrow K^0 (K^{*0})$ for $q = d$; $B_s^0 \rightarrow \eta, \eta' (\phi)$ for $q = s$; $B_c^+ \rightarrow D_s^+ (D_s^{*+})$ for $q = c$; and $\eta_b \rightarrow \overline{B_s^0} (\overline{B_s^{*0}})$ for $q = b$.
- The operators with $q_j = s$ and $q_i = d$ trigger $K^0 \rightarrow NN$ and $K^0 \rightarrow \nu N$ decays, as well as the following transitions: $K^+ \rightarrow \pi^+$ for $q = u$; $K^0 \rightarrow \pi^0$ for $q = d$; $\eta' \rightarrow \overline{K^0} (\overline{K^{*0}})$ for $q = s$; $D_s^+ \rightarrow D^+$ for $q = c$; and $\overline{B_s^0} \rightarrow \overline{B^0} (\overline{B^{*0}})$ for $q = b$. We will not consider these decay modes in what follows. This is because for the listed D_s^+ and $\overline{B_s^0}$ decays, the available mass window is very small, and for the light mesons' decays (kaons and η'), the numerical predictions from Pythia8 [60, 61], which we will use for numerical simulation in this work, do not agree well with the LHCf experiment [62].

We have computed the corresponding partial decay widths assuming both N and ν are (i) Dirac and (ii) Majorana particles. In appendix A, we provide the formulae for the two-body decay widths and the three-body decay amplitudes in both cases. To compute the three-body decay widths, we have used the procedure described in Ref. [17]. We summarize it in appendix A.2 for completeness.

⁶This condition is necessary, but not sufficient, since a meson mass is not a simple sum of the masses of its constituent quarks.

⁷In the case of Dirac ν and N , these decays should read $D^0 \rightarrow N\overline{N}$ and $D^0 \rightarrow \nu\overline{N}$ ($D^0 \rightarrow \overline{\nu}N$).

⁸In figure 1, we need to send $\bar{q} \rightarrow q$ and $q_{j,i} \rightarrow \bar{q}_{j,i}$ to match the particle content of B -mesons.

Decay	Limit on BR	Decay	Limit on BR	Decay	Limit on BR
$D^0 \rightarrow \text{inv.}$	9.4×10^{-5}	$B^0 \rightarrow \text{inv.}$	2.4×10^{-5}	$B_s^0 \rightarrow \phi \nu \bar{\nu}$	5.4×10^{-3}
		$B^0 \rightarrow \pi^0 \nu \bar{\nu}$	9.0×10^{-6}	$B^0 \rightarrow K^0 \nu \bar{\nu}$	2.6×10^{-5}
		$B^0 \rightarrow \rho^0 \nu \bar{\nu}$	4.0×10^{-5}	$B^0 \rightarrow K^{*0} \nu \bar{\nu}$	1.8×10^{-5}
		$B^+ \rightarrow \pi^+ \nu \bar{\nu}$	1.4×10^{-5}	$B^+ \rightarrow K^+ \nu \bar{\nu}$	1.6×10^{-5}
		$B^+ \rightarrow \rho^+ \nu \bar{\nu}$	3.0×10^{-5}	$B^+ \rightarrow K^{*+} \nu \bar{\nu}$	4.0×10^{-5}

Table 5. Upper limits on the branching ratios (BRs) of (semi-)invisible D - and B -meson decays extracted from Ref. [58]. The limits highlighted in bold provide the most stringent constraints on the corresponding Wilson coefficients, see section 5.

If the products of HNL decays are not detected, the modes we consider here contribute to the $P \rightarrow \text{inv.}$ or $P \rightarrow P'/V \nu \bar{\nu}$ decays. The existing upper limits on the branching ratios of such decays are listed in table 5. In what follows, we will take these constraints into account.

In figure 2, we show the branching ratios of D - and B -meson decays induced by the LNC pair- N_R operators $\mathcal{O}_{uN,12}^{V,RR}$ (top), $\mathcal{O}_{dN,31}^{V,RR}$ (middle) and $\mathcal{O}_{dN,32}^{V,RR}$ (bottom), assuming N is Majorana. We turn on one operator at a time, setting the corresponding Wilson coefficient to $10^{-3}v^{-2}$. This choice allows us to avoid the bounds from (semi-)invisible meson decays summarized in table 5. We see that the two-body decay dominates over the three-body ones for $m_N \gtrsim 325$ MeV in the case of $\mathcal{O}_{uN,12}^{V,RR}$, for $m_N \gtrsim 1.2$ GeV in the case of $\mathcal{O}_{dN,31}^{V,RR}$, and for $m_N \gtrsim 1.05$ GeV in the case of $\mathcal{O}_{dN,32}^{V,RR}$. For small m_N , the two-body decay is suppressed, since the corresponding decay width is proportional to m_N^2 , see Eq. (A.13) in appendix A. Turning on the LR operators $\mathcal{O}_{uN,12}^{V,LR}$, $\mathcal{O}_{dN,31}^{V,LR}$, and $\mathcal{O}_{dN,32}^{V,LR}$ (one at a time) would lead to the same results as can be seen from Eqs. (A.13), (A.24) and (A.25).

In figure 3, we display the branching ratios of the same meson decays, but this time triggered by the LNV pair- N_R operators $\mathcal{O}_{uN,12}^{S,RR}$ (top), $\mathcal{O}_{dN,31}^{S,RR}$ (middle), and $\mathcal{O}_{dN,32}^{S,RR}$ (bottom). Again, we turn on one operator at a time and set the corresponding Wilson coefficient to $10^{-3}v^{-2}$.⁹ Contrary to the LNC operators, now the leptonic two-body decays dominate for all kinematically available values of m_N , since there is no helicity suppression from m_N , cf. Eq. (A.13). Switching on the LR operators $\mathcal{O}_{uN,12}^{S,LR}$, $\mathcal{O}_{dN,31}^{S,LR}$, and $\mathcal{O}_{dN,32}^{S,LR}$ (one at a time) would lead to the same results as can be inferred from Eqs. (A.13), (A.24), and (A.25). The tensor operators $\mathcal{O}_{dN}^{T,RR}$ and $\mathcal{O}_{uN}^{T,RR}$ vanish identically for one generation of N_R . For this reason, we do not consider them in what follows.

Concerning single- N_R operators, we have also studied their contribution to two- and three-body D - and B -meson decays, showing some results in appendix B. In particular, we

⁹In the case of non-hermitian operators, as *e.g.* $\mathcal{O}_{qN}^{S,RR}$, $q = u$ or d , “one operator at a time” means $c_{qN,ij}^{S,RR} \neq 0$, whereas $c_{qN,ji}^{S,RR} = 0$. We note also that $c_{dN,31}^{S,RR} = 10^{-3}v^{-2}$ violates slightly the limit on $\text{BR}(B^0 \rightarrow \text{inv.})$ from table 5. However, we opt for this value of the Wilson coefficient to be uniform with the other plots.

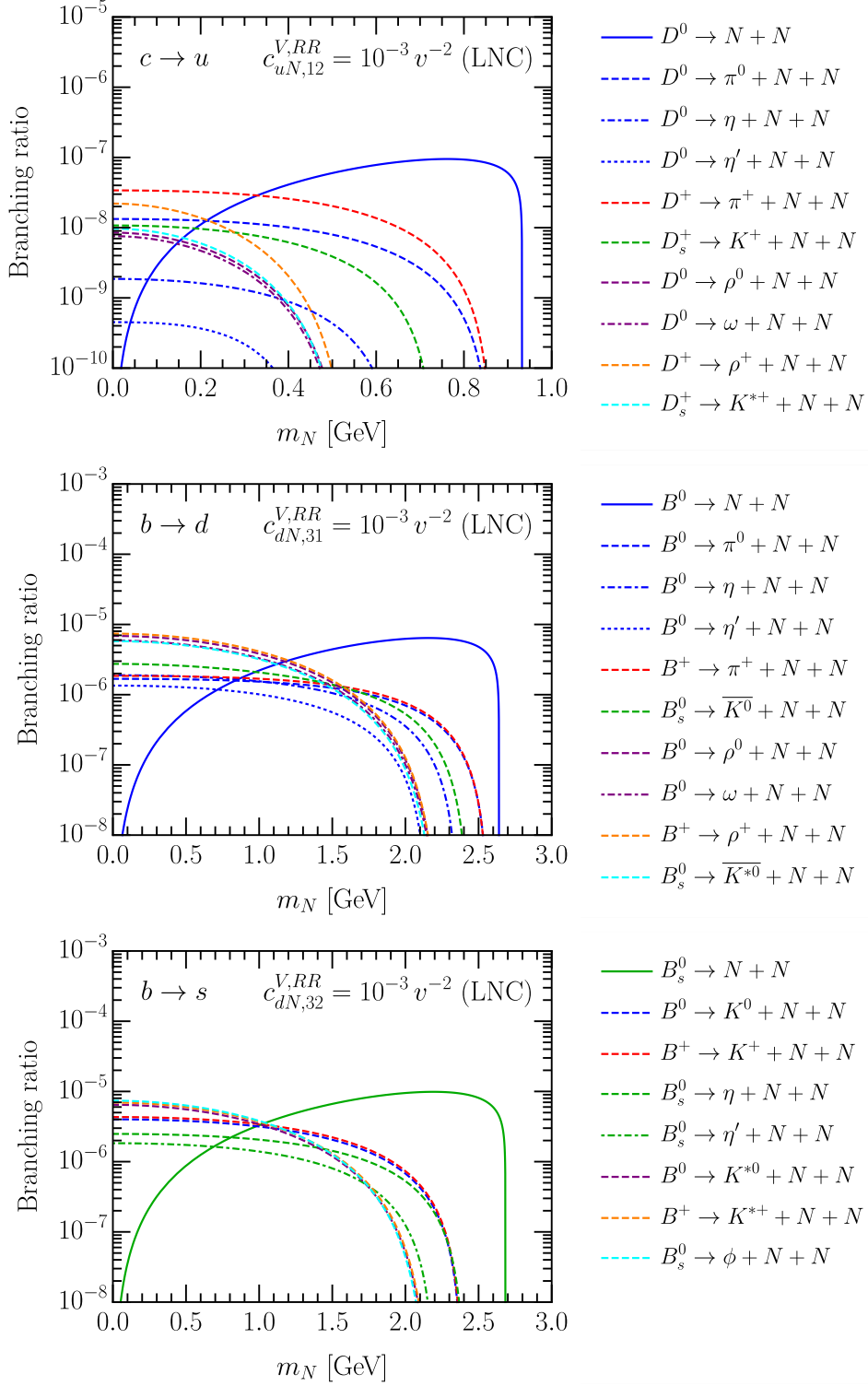


Figure 2. Branching ratios of D - and B -meson decays triggered by the LNC pair- N_R operators $\mathcal{O}_{uN,12}^{V,RR}$ (top), $\mathcal{O}_{dN,31}^{V,RR}$ (middle) and $\mathcal{O}_{dN,32}^{V,RR}$ (bottom). The corresponding Wilson coefficient has been set to $10^{-3}v^{-2}$.

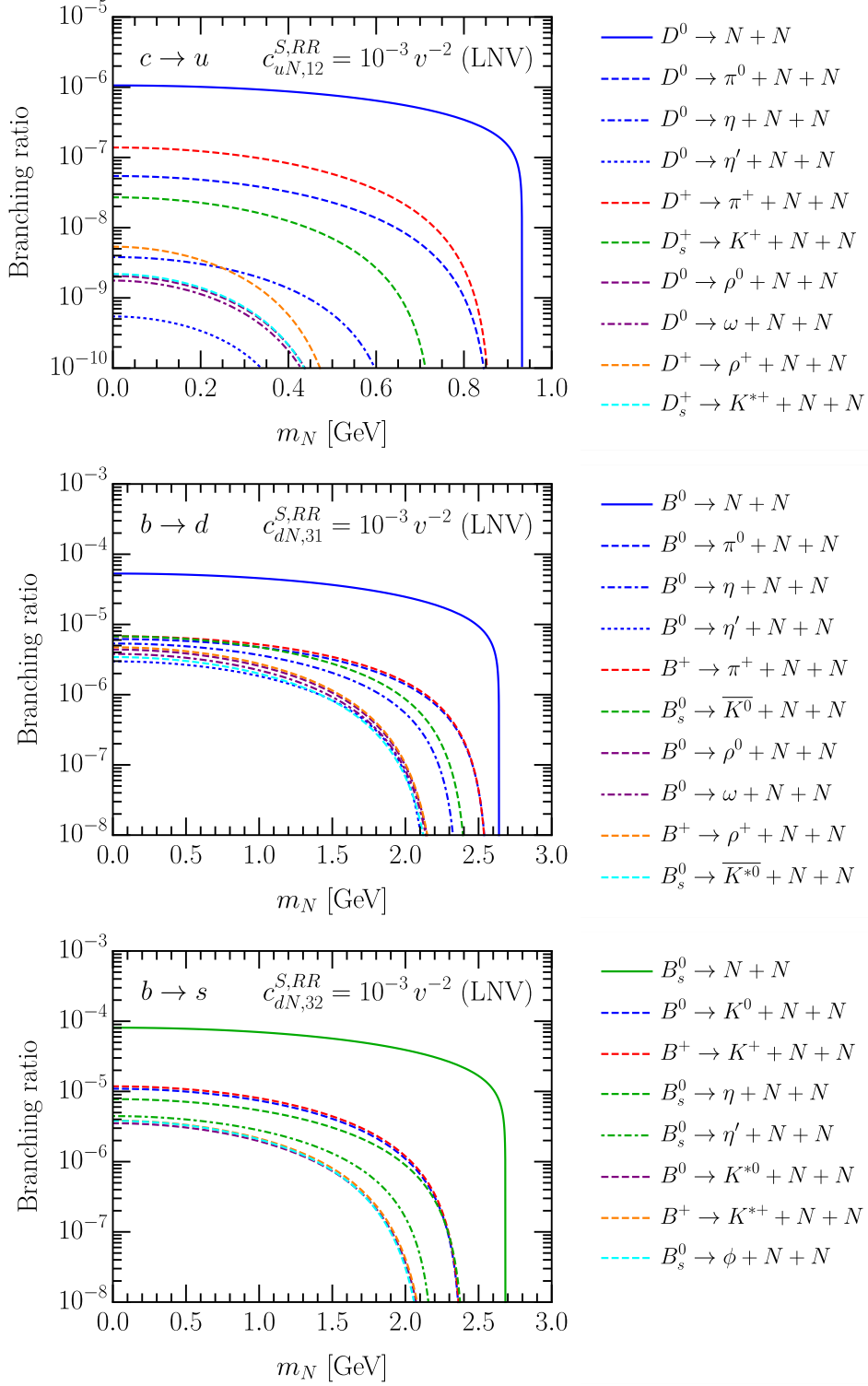


Figure 3. Branching ratios of D - and B -meson decays triggered by the LNV pair- N_R operators $\mathcal{O}_{uN,12}^{S,RR}$ (top), $\mathcal{O}_{dN,31}^{S,RR}$ (middle) and $\mathcal{O}_{dN,32}^{S,RR}$ (bottom). The corresponding Wilson coefficient has been set to $10^{-3}v^{-2}$.

present in figure 8 the branching ratios of B -meson decays induced by the LNC operators $\mathcal{O}_{d\nu N,31\alpha}^{S,RR}$ and $\mathcal{O}_{d\nu N,31\alpha}^{T,RR}$ and the LNV operator $\mathcal{O}_{d\nu N,31\alpha}^{V,RR}$. We observe that our results are analogous to the ones obtained in Ref. [17], cf. figure 2 therein, for single- N_R operators including a charged lepton. Therefore, we expect the constraints derived from the far detectors to be essentially the same for the neutral-current single- N_R operators, and we hence do not include the latter in our numerical simulation.

Before closing the section, we mention that with only one N_R generation, pair- N_R operators cannot make the HNL decay by themselves, in contrast to single- N_R operators. In appendix C, we have computed the partial decay widths of HNLs into a light meson and an active neutrino triggered by the neutral single- N_R operators. Since we only simulate HNLs produced by pair- N_R operators and only turn on one N_R LEFT operator at a time, we consider that the HNL decay is exclusively due to active-heavy neutrino mixing. The partial decay widths of HNL via mixing are computed according to the formulae given in Refs. [17, 55, 63].

4 Experiments and details of simulation

In this work, we focus on a series of far-detector experiments proposed or even approved at the LHC. These programs were mostly proposed in recent years and include ANUBIS [3], AL3X [4], CODEX-b [5], FACET [6], FASER and FASER2 [7, 8], MAPP1 and MAPP2 [9, 10], and MATHUSLA [2, 11, 12]. Since they are supposed to be operated at different interaction points (IPs) and time scales of the LHC, the projected integrated luminosities also vary, ranging from as low as 30 fb^{-1} for MAPP1, up to the full HL-LHC target, 3 ab^{-1} for ANUBIS, FACET, FASER2, and MATHUSLA. Moreover, typically these far detectors are located with a distance of $\mathcal{O}(1) - \mathcal{O}(100)$ m to their corresponding IP, allowing for sufficient amount of rock, lead, or other shielding material to effectively remove the potential SM background events stemming from the IP. As a result, vanishing background is usually assumed for phenomenological studies on these experiments.

Here, we study HNLs pair-produced at the LHC with the center-of-mass energy $\sqrt{s} = 14 \text{ TeV}$ from charm and bottom mesons' rare decays mediated by a N_R LEFT operator. These HNLs then travel a certain distance before decaying via their mixing with the SM active neutrino. If the boosted decay length of the HNLs falls into a suitable range, the HNLs have a high probability of decaying inside some of the far detectors. Since the HNLs mostly decay to channels that are not fully invisible (three active neutrinos), the decay vertex can be reconstructed by these experiments.

While we analytically compute the production and decay rates of the HNLs, we rely on a Monte-Carlo simulation tool, Pythia8.3 [60, 61], to estimate the decay probabilities of the HNLs inside each of the far detectors. Depending on the flavor indices of the EFT operator we choose to turn on, Pythia8 can generate either the $pp \rightarrow c\bar{c}$ or $pp \rightarrow b\bar{b}$ process inclusively for D - or B -meson production at the LHC, respectively. These mesons then decay to different channels including at least two HNLs, with relative decay branching

D^0	D^\pm	D_s^\pm	B^0	B^\pm	B_s^0
4.12×10^{16}	2.16×10^{16}	7.02×10^{15}	1.58×10^{15}	1.58×10^{15}	2.73×10^{14}

Table 6. Inclusive production numbers of D - and B -mesons for an integrated luminosity of 3 ab^{-1} , extracted from Ref. [17], but multiplied by a factor of 1.08 (1.06) for the B -mesons (D -mesons) obtained with Pythia8 to account for the increase in production cross section of the heavy mesons from the center-of-mass energy 13 TeV to 14 TeV [16].

ratios implemented according to the analytical computation detailed in section 3. This allows for maximal usage of all the simulated data while respecting the relative importance of each decay channel. Since Pythia8 provides the kinematics of each simulated HNL, we can compute its decay probability in each detector according to the geometry and position with respect to the IP. We then take the average of the decay probabilities of all the simulated HNLs, to obtain the expected acceptance rate at each detector, $\langle P[N \text{ decay}] \rangle$. This allows us to compute the projected number of signal events, N_S , with the following equation:

$$N_S = \sum_i 2 \cdot N_{M_i} \cdot \text{BR}(M_i \rightarrow NN + \text{anything}) \cdot \langle P[N \text{ decay}] \rangle \cdot \text{BR}(N \rightarrow \text{vis.}), \quad (4.1)$$

where the factor 2 accounts for the fact that each decay of the mesons into the HNLs via the $N_{R\text{LEFT}}$ operator includes two HNLs, N_{M_i} is the number of the mother mesons, and $\text{BR}(N \rightarrow \text{vis.})$ denotes the decay branching ratio of the HNLs into visible final states. For our study, we consider only the decay channel into three active neutrinos to be invisible.

In table 6, we reproduce the inclusive production rates of all the relevant types of heavy mesons from Ref. [17], which were obtained therein combining both LHCb measurements and extrapolation with the state-of-the-art simulation tools FONLL [64, 65] and Pythia8. Note that in table 6 we have in addition multiplied the production rates of these heavy mesons given in Ref. [17] by a factor of 1.08 and 1.06 for the B - and D -mesons, respectively, in order to take into account the fact that we consider $\sqrt{s} = 14 \text{ TeV}$ instead of 13 TeV [16].

In principle, the computation of the decay probability of each HNL can be summarized with a simple formula, if the flight path of the HNL traverses the detector:

$$P[N \text{ decay}] = e^{-L_1/\beta\gamma c\tau} - e^{-L_2/\beta\gamma c\tau}, \quad (4.2)$$

where β , γ , and τ are the speed, Lorentz boost factor, and the proper lifetime of the HNL, c is the speed of light, and L_1 and L_2 label respectively the distance from the IP (where we assume the heavy mesons decay into the HNLs instantly) to the incoming and outgoing sides of the detector. This formula holds perfectly for a far detector with a spherical-shell shape facing towards the IP. However, since the far-detector experiments mostly have a more complicated geometrical shape and relative orientation with respect to the IP, more sophisticated formulae are required for more accurate estimate of the decay probability. In this paper, we strictly follow Ref. [17] for computing the decay probabilities in each far

detector with the corresponding geometrical configuration. As exception, FACET [6] was not included in Ref. [17], so here, we give a brief description of this detector. Its concept is essentially rather similar to that of FASER(2) and AL3X. It is a proposed cylindrical detector in the forward direction of the CMS experiment, with a distance of 101 m between the CMS IP and its near end. Further, it has a radius of 0.5 m and length 18 m. However, it does not cover the pseudorapidity up to infinity as FASER(2) does; instead, it covers the polar angle between 1 and 4 mrad, or equivalently, the pseudorapidity between 6.2 and 7.6. We require that the HNLs travel towards the far end of the FACET decay chamber (but not to the sides).

Before closing, we should also mention that since Pythia8 is not well validated for heavy meson production in the very forward direction, we use FONLL to correct the differential production cross section of mesons for various ranges of small transverse momentum and large pseudorapidity, for three experiments: FACET, FASER, and FASER2.

5 Results of numerical analysis

We present and discuss the numerical results in this section. We restrict ourselves to Majorana HNLs, and study the LNC and LNV pair- N_R operators in the $N_{R\text{LEFT}}$ triggering the meson decays described in section 3. More specifically, the set of the LNC operators we consider is $\mathcal{O}_{uN,12}^{V,RR}$, $\mathcal{O}_{dN,31}^{V,RR}$, and $\mathcal{O}_{dN,32}^{V,RR}$, and the set of the LNV operators is $\mathcal{O}_{uN,12}^{S,RR}$, $\mathcal{O}_{dN,31}^{S,RR}$, and $\mathcal{O}_{dN,32}^{S,RR}$.¹⁰ We first show in figures 4 and 5 sensitivity reaches of the various far detectors we consider, in the plane $|V_{lN}|^2$ vs. m_N , for the LNC and LNV operators, respectively. These isocurves are for three signal events, corresponding to 95% confidence level (C.L.) limits, given zero background events. We switch on one operator only each time and fix the corresponding Wilson coefficient to $10^{-3}v^{-2}$, where $v = 246$ GeV is the SM Higgs VEV. This is approximately 700 times smaller than the Fermi constant and, for the LNC operators, corresponds to a NP scale Λ_{NP} of 7.78 TeV for $c \sim 1/\Lambda_{\text{NP}}^2$. For this value of the Wilson coefficient, the limits coming from the D^0 and B^0 invisible decays, as well as from $P \rightarrow P'/V\nu\bar{\nu}$, are avoided (see section 3). In our numerical simulation, we consider the HNLs only dominantly mixing with either the electron neutrino or the muon neutrino: $l = e, \mu$. We do not consider HNLs decaying to τ 's, because we expect the sensitivities to be much reduced, compared to e, μ .

In figure 4, we observe that in the top-right and bottom-left plots, there is stronger reach in m_N than in the top-left plot. This is due to the larger masses of B -mesons than those of D -mesons and hence higher kinematic thresholds. Moreover, the B -meson scenarios show better exclusion limits in $|V_{lN}|^2$ as well, compared to the D -meson one, despite the larger production rates of D -mesons than those of B -mesons by about one order of magnitude, cf. table 6. The main reason is that the decay branching ratios of

¹⁰We recall that the corresponding LR operators, if switched on one at a time, would lead to the same results.

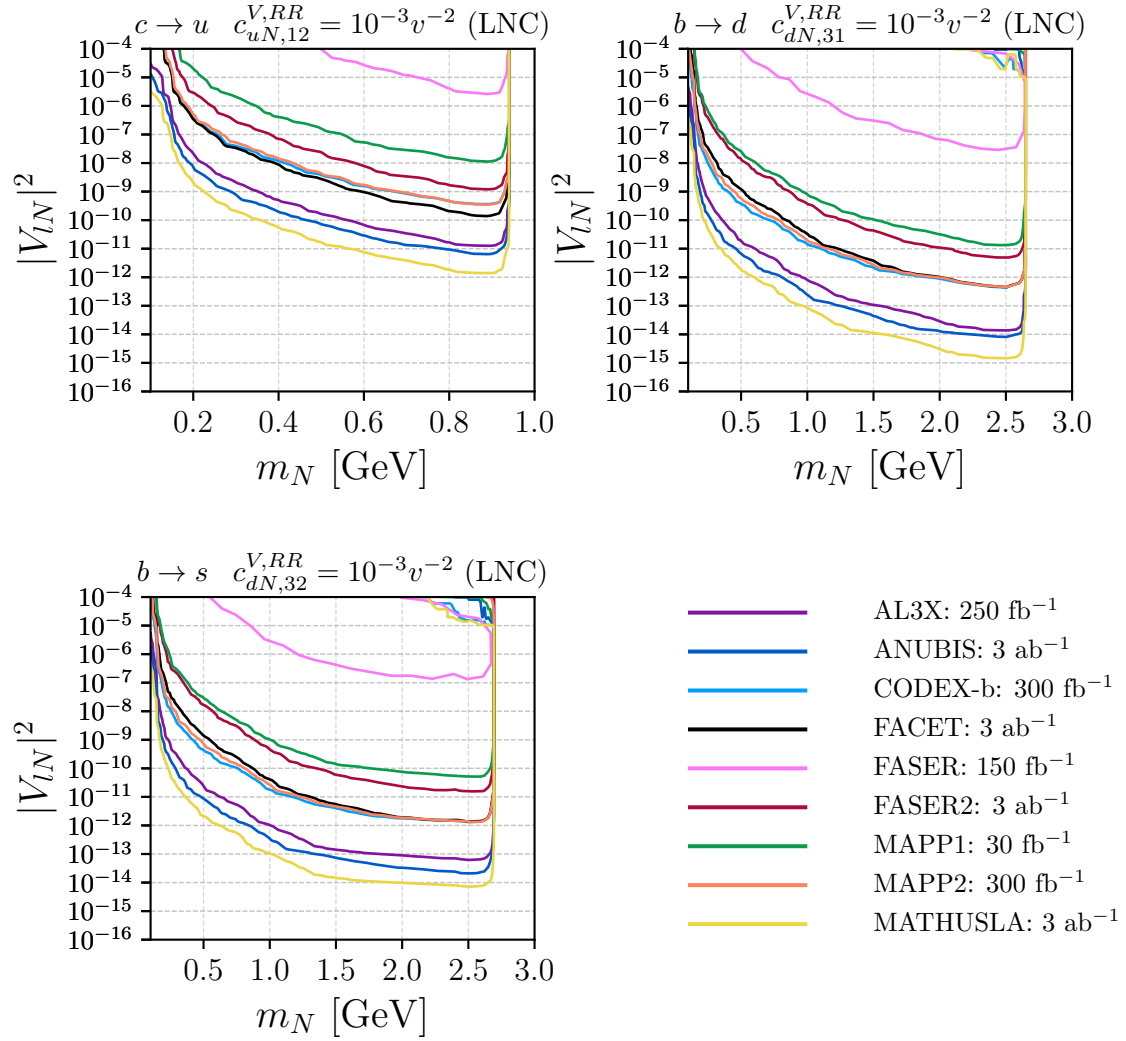


Figure 4. Exclusion limits in the plane $|V_{lN}|^2$ vs. m_N , for the three LNC pair- N_R operators we consider, with the corresponding Wilson coefficients fixed to $10^{-3}v^{-2}$.

B -mesons into the HNLs are in general larger than those of D -mesons by about two orders of magnitude, cf. figure 2, assuming equal values of the corresponding Wilson coefficients.

Among these far-detector experiments, we find the best limits come from MATHUSLA, which can probe the values of $|V_{lN}|^2$ down to 10^{-12} (10^{-15}) in the charm (bottom) scenario(s), followed by ANUBIS and AL3X, while FASER shows the weakest sensitivities, mainly because of its small volume. We note that the approved experiment MAPP1 with only 30 fb^{-1} of integrated luminosity can already compete with the future experiment FASER2 with the full HL-LHC data, especially in the bottom scenarios. The reason is its larger size and smaller distance to the corresponding IP. Also, CODEX-b, MAPP2, and FACET can exclude almost the same parts of the parameter space.

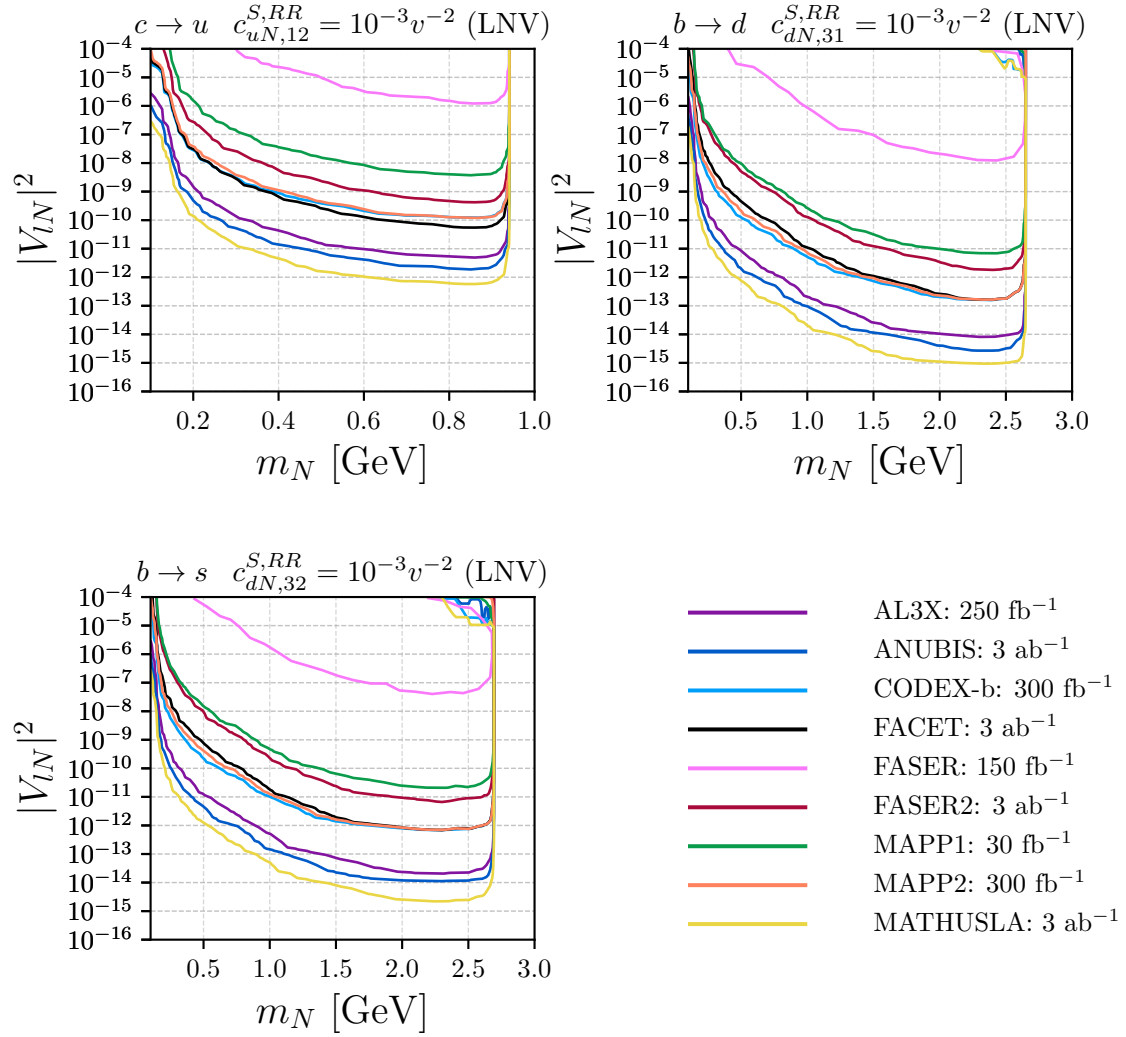


Figure 5. The same plots as Fig. 4, but for the three LNV pair- N_R operators.

The plots in figure 5 are very similar to those in figure 4, with the main difference being that the exclusion limits in $|V_{lN}|^2$ are slightly stronger because the decay branching ratios of the mesons into a pair of HNLs are larger in the LNV case than in the LNC case, given the same value of the Wilson coefficients, see figures 2 and 3.

The best present limits for HNL masses below 5 GeV that can be found in the literature come from different experiments such as NA62 [66], T2K [67], CHARM [68], PS191 [69], JINR [70], Belle [71], and DELPHI [72]. These limits are around $|V_{lN}|^2 \sim 10^{-9}$ – 10^{-5} , depending on the HNL mass, and correspond to a minimal HNL scenario in which both the production and the decay of the HNL are determined by their mixing with the active neutrinos. In our theoretical setup, however, the production of the HNLs receives additional contributions from effective operators affecting the HNL sensitivity of these experiments.

A detailed reinterpretation of the current HNL limits coming from different experiments in the N_R LEFT depends on specific details of each particular experiment, and it is beyond the scope of this current work. For this reason, we do not show these bounds in figures 4 and 5.

We then present in figures 6 and 7 the sensitivity curves in the plane c vs. m_N , for two fixed values of active-heavy mixing, $|V_{lN}|^2 = 10^{-7}$ and $|V_{lN}|^2 = 10^{-10}$. In order to obtain these plots, we select the chosen benchmark mixing parameters and find the value of the Wilson coefficient in each scenario such that the predicted number of signal events is equal to three. We find the same hierarchy in sensitivities of these experiments as in figures 4 and 5, but the final reaches in c differ between the two chosen $|V_{lN}|^2$ values. This is because for any fixed HNL mass, varying the mixing parameter squared would change the proper lifetime of the HNL and hence the detectors' acceptance to these HNLs. $|V_{lN}|^2 = 10^{-7}$ corresponds to an acceptance rate roughly three orders of magnitude better than that given by $|V_{lN}|^2 = 10^{-10}$, in the large decay length limit ($\beta\gamma c\tau \gg L_1, L_2$, as in Eq. (4.2)). Therefore, the lower sensitivity reach in c for $|V_{lN}|^2 = 10^{-10}$ is roughly weaker than that for $|V_{lN}|^2 = 10^{-7}$, by a factor of $\sqrt{1000} \approx 32$, since the HNL production rates are proportional to c^2 . In the charm scenario, for the larger mixing parameter case, we find the best experiments (MATHUSLA, ANUBIS, and AL3X) can reach c as low as about 10^{-4} TeV $^{-2}$, while the other weaker experiments can still probe c down to the order of 10^{-3} TeV $^{-2}$ except FASER, or even better by about one order of magnitude in the two bottom scenarios. In the LNC case, $c \sim 10^{-4}$ (10^{-5}) TeV $^{-2}$ corresponds roughly to a new physics scale Λ_{NP} of 100 (316) TeV, if we take $c \sim 1/\Lambda_{\text{NP}}^2$ and ignore the relatively minor effects of QCD running.

Again as in figures 4 and 5, we find the LNV results in figure 7 are slightly stronger than the LNC ones in figure 6, for the same reason as stated above. Here, the conversion from Wilson coefficient to Λ_{NP} is more subtle than the LNC operators' case, because the $d = 6$ LNV operators at the scale below $v = 246$ GeV are matched to the $d = 7$ operators that include a Higgs boson in the N_R SMEFT, cf. Eq. (2.10). Therefore, we estimate that for $c \sim 10^{-4}$ (10^{-5}) TeV $^{-2}$ in the low energy scale, the corresponding Λ_{NP} is about 10 (21) TeV, with $c \sim v/(2\sqrt{2}\Lambda_{\text{NP}}^3)$, if we again ignore the QCD running effects. This is weaker than the LNC case by about one order of magnitude.

The gray shaded regions in figures 6 and 7 correspond to the limits coming from invisible and semi-invisible D - and B -meson decays collected in table 5. More specifically, in the $c \rightarrow u$ scenario, it is $D^0 \rightarrow \text{inv.}$ which provides the only constraint. In the $b \rightarrow d$ scenario and for the LNC operator (middle-row plots in figure 6), there is an interplay between $B^0 \rightarrow \pi^0 \nu \bar{\nu}$, which dominates for $m_N \lesssim 1.3$ GeV, and $B^0 \rightarrow \text{inv.}$, which takes over for larger HNL masses. For the LNV operator (figure 7), $B^0 \rightarrow \text{inv.}$ provides the most stringent constraint for any kinematically allowed m_N . Finally, in the $b \rightarrow s$ scenario, the leading bound originates from the limit on the branching ratio of $B^+ \rightarrow K^+ \nu \bar{\nu}$. All these bounds have been derived by equating $\text{BR}(P \rightarrow NN)$ ($\text{BR}(P \rightarrow P' NN)$) obtained using Eq. (A.13) (Eq. (A.24)) to the corresponding upper limit on $\text{BR}(P \rightarrow \text{inv.})$ ($\text{BR}(P \rightarrow P' \nu \bar{\nu})$) from

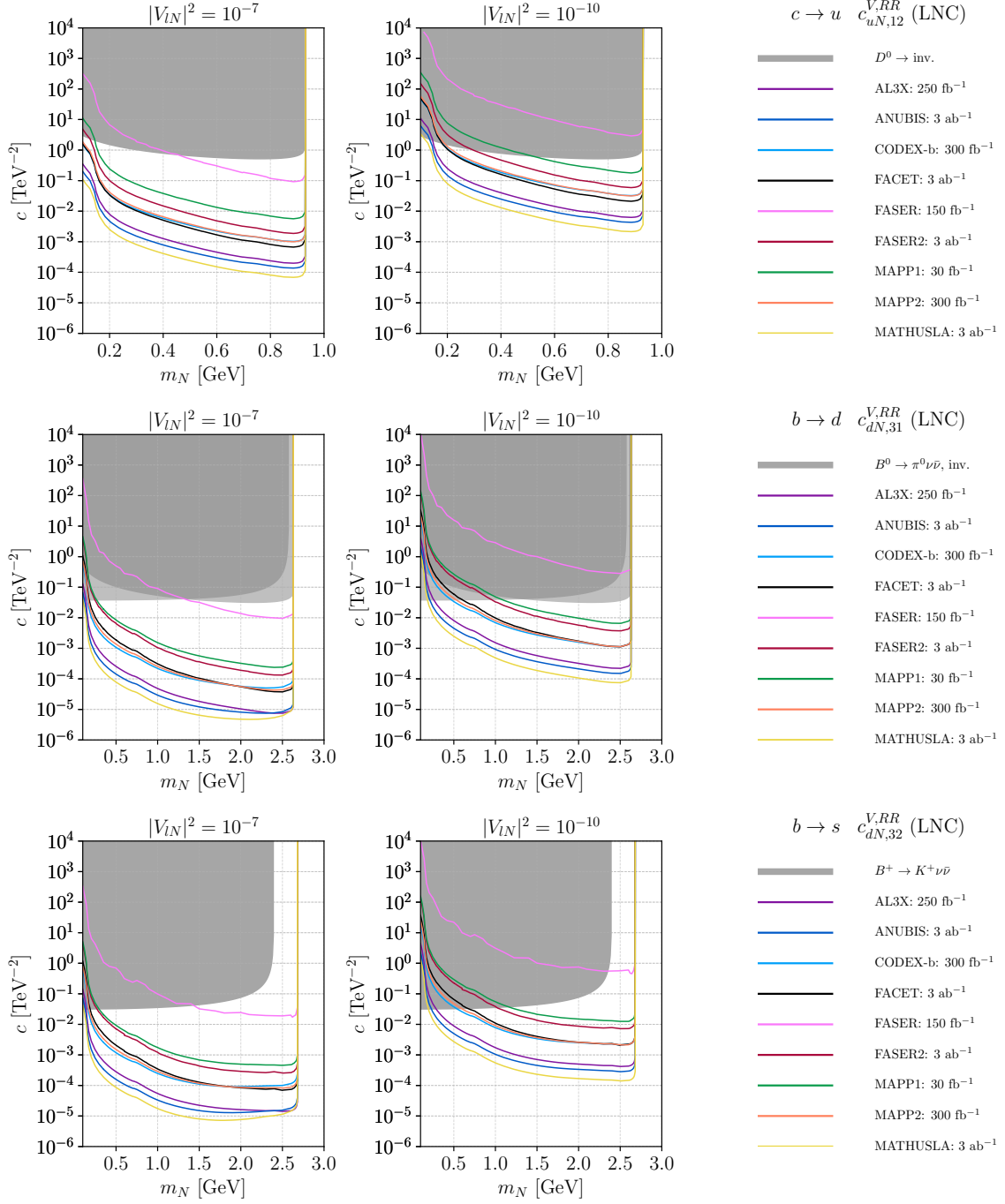


Figure 6. Exclusion limits in the plane c vs. m_N , for the three LNC pair- N_R operators we consider, with $|V_{lN}|^2$ fixed at 10^{-7} or 10^{-10} .

table 5.

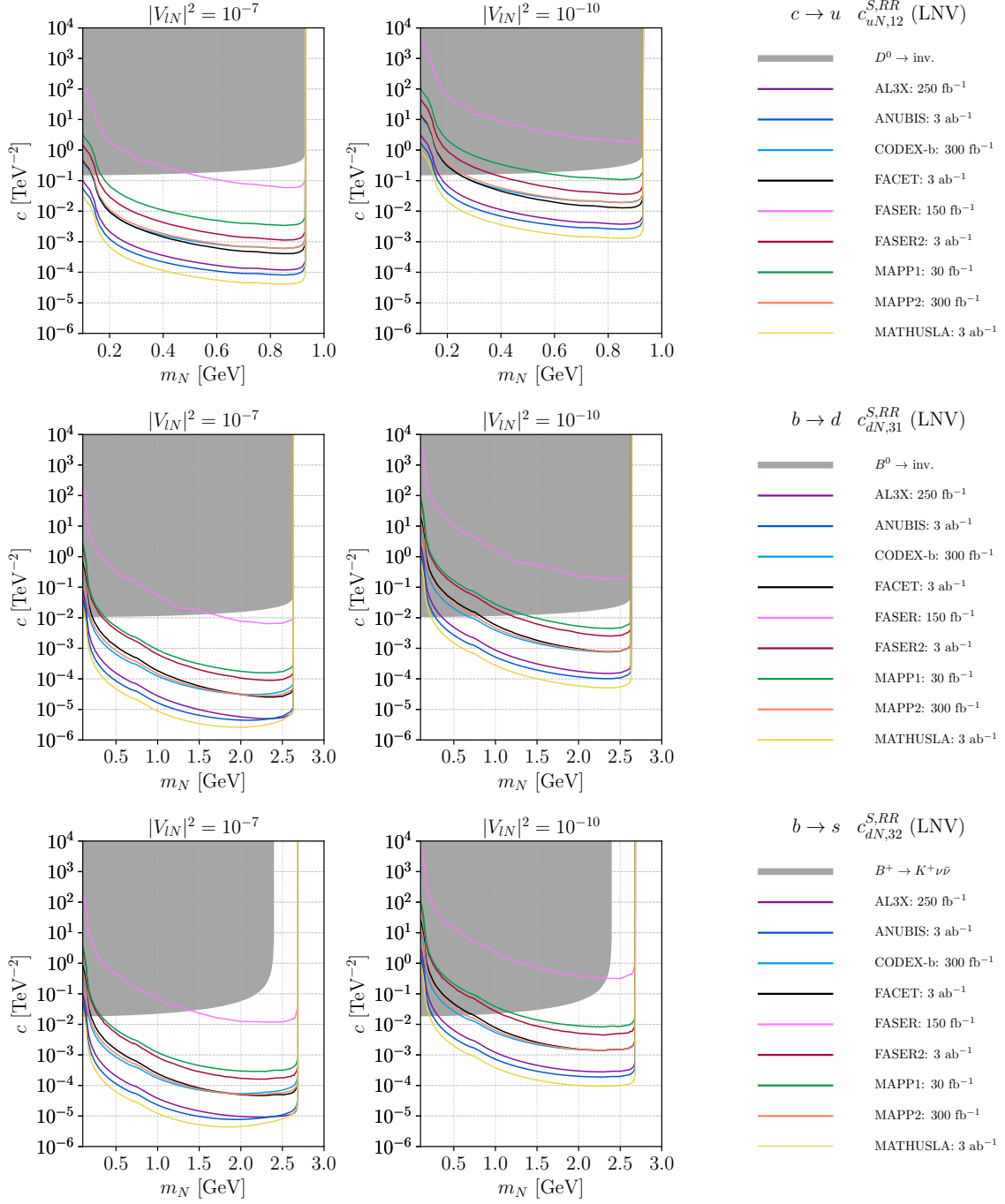


Figure 7. The same plots as Fig. 6, but for the three LNV pair- N_R operators.

6 Summary and conclusions

In this work, we have focused on dimension-6 operators involving a pair of heavy neutral leptons (HNLs), in the framework of the low-energy effective field theory of the Stan-

standard Model extended with HNLs (N_R LEFT). We have considered both lepton-number-conserving (LNC) and lepton-number-violating (LNV) operators. Such operators with certain quark-flavor combinations can lead to charm and bottom meson decays into a pair of HNLs, in either two-body or three-body decays. We have considered three combinations of the quark flavor indices, leading to the $c \rightarrow u$, $b \rightarrow d$, and $b \rightarrow s$ transitions, and computed the corresponding production rates of the HNL pair from various D - and B -meson decays for (i) the LNC operators $\mathcal{O}_{uN,12}^{V,RR}$, $\mathcal{O}_{dN,31}^{V,RR}$, and $\mathcal{O}_{dN,32}^{V,RR}$, and (ii) the LNV operators $\mathcal{O}_{uN,12}^{S,RR}$, $\mathcal{O}_{dN,31}^{S,RR}$, and $\mathcal{O}_{dN,32}^{S,RR}$. The corresponding decay branching ratios for both LNC and LNV cases are shown in figures 2 and 3, respectively. Switching on the corresponding LR operators (one at a time) would lead to the same results. It is interesting to observe that for the LNC case, the mesons' three-body and two-body decays are dominant, respectively, for relatively lower and higher masses in the kinematically allowed range of the HNL mass, for all three quark-flavor scenarios. On the other hand, for the LNV case, the two-body decays are the most important channel for the whole kinematically relevant mass range.

Since these operators entail a pair of HNLs and in the absence of other effective interactions, HNLs can decay only via an additional HNL mixing with the active neutrinos in the weak current.¹¹ Therefore, we study HNL production from the EFT operators, and HNL decays through active-heavy neutrino mixing. Since we focus on GeV-scale HNLs, small neutrino mixing parameters naturally lead these HNLs to become long-lived. Here, we choose therefore to consider a series of far-detector proposals at the LHC. These include AL3X, ANUBIS, CODEX-b, FACET, FASER and FASER2, MAPP1 and MAPP2, and MATHUSLA. These experiments have been proposed (some even approved and operated) mainly for searching for long-lived particles (LLPs) and would be constructed with a distance of about 5–500 meters away from different interaction points (IPs). With shielding materials on site between a far detector and its corresponding IP, such experiments are usually assumed to be background-free for LLP searches.

We then perform Monte-Carlo simulation with the tool Pythia8, to estimate the acceptance rates of these far detectors for HNLs pair-produced from D - and B -meson decays. For small mixing and mass, these HNLs are long-lived and decay outside the LHC main detectors. With the total production rates of the mesons at the LHC in knowledge, we can estimate the number of HNL decays in the far detectors, using decay width formulae for (i) the HNL production from meson decays in the N_R LEFT, and (ii) the HNL decays via their mixing with the active neutrinos. For simplicity, we consider the HNLs to be mixed with only either the electron neutrino or the muon neutrino. Further, for the signal, we consider only the HNL decays into three active neutrinos to be invisible; all the other decay channels are included as signature.

We show our numerical results in two types of planes: $|V_{lN}|^2$ vs. m_N in figures 4 and 5, and c vs. m_N in figures 6 and 7. For all these results, we consider both LNC and LNV dimension-six operators, for all three quark-flavor scenarios. In general, we find the

¹¹Actually, an HNL can also decay through a pair- N_R operator in conjunction with mixing, but such decays are suppressed compared to the decays through mixing alone.

constraints on the LNV operators to be slightly stronger than those on the LNC ones, because the meson decay branching ratios into HNLs in the LNV case are larger by about one order of magnitude than those in the LNC case (for the same value of the corresponding Wilson coefficients); see figures 2 and 3.

Among all the studied far detectors, we find MATHUSLA, ANUBIS, and AL3X show the best sensitivities, while FASER is usually the weakest. Compared to FASER2, MAPP1 achieves very similar results with 100 times less data, mainly as a result of its much larger volume and closer distance to the IP.

In the $|V_{lN}|^2$ vs. m_N plots, we find these experiments can probe $|V_{lN}|^2$ as low as 10^{-15} – 10^{-6} , for GeV-scale HNLs. Then, for two fixed benchmark values of $|V_{lN}|^2 = 10^{-7}$ and $|V_{lN}|^2 = 10^{-10}$, we obtain the sensitivity reach in the Wilson coefficients c as functions of the HNL mass, for these far-detector experiments. We further convert c to the new-physics (NP) scale Λ_{NP} . We find for $|V_{lN}|^2 = 10^{-7}$, the considered experiments can probe the NP scale up to between approximately 10 and several hundred TeV depending on the type of the operator considered, while for $|V_{lN}|^2 = 10^{-10}$, the reach in Λ_{NP} is reduced by slightly less than one order of magnitude, as a result of the larger decay length and hence smaller acceptance.

Acknowledgements

This work is supported by the Spanish grants PID2020-113775GB-I00 (AEI/10.13039/501100011033) and CIPROM/2021/054 (Generalitat Valenciana). R.B. acknowledges financial support from the Generalitat Valenciana (grant ACIF/2021/052). G.C. acknowledges support from ANID FONDECYT grant No. 11220237. G.C. and J.C.H. also acknowledge support from ANID FONDECYT grant No. 1201673 and ANID – Millennium Science Initiative Program ICN2019_044. The work of A.T. is supported by the “Generalitat Valenciana” under the grant PROMETEO/2019/087 and by the MICINN-AEI (10.13039/501100011033) grant PID2020-113334GB-I00. Z.S.W. is supported by the Ministry of Science and Technology (MoST) of Taiwan with grant number MoST-110-2811-M-007-542-MY3.

A Pseudoscalar meson decays into HNLs

The four-fermion interactions described by the $N_R\text{LEFT}$ operators in tables 1 and 2 lead to two-body and three-body meson decays, if the HNL mass is small enough. The former involve two neutral leptons in the final state, whereas the latter correspond to semileptonic decays with an additional lighter meson within the final products. This appendix gathers the necessary formulae to determine meson decay rates into HNLs, assuming a pseudoscalar meson (of mass m_P and momentum p) in the initial state.

In pure leptonic decays we define the meson decay constants through the transition matrix elements (see *e.g.* Ref. [17]):

$$\begin{aligned}\langle 0 | \bar{q}_i \gamma^\mu \gamma_5 q_j | P(p) \rangle &= i f_P p^\mu, \\ \langle 0 | \bar{q}_i \gamma_5 q_j | P(p) \rangle &= i \frac{m_P^2}{m_{q_i} + m_{q_j}} f_P \equiv i f_P^S,\end{aligned}\tag{A.1}$$

where i, j denote quark flavor indices, and $|P(p)\rangle$ is the decaying pseudoscalar meson.

In semileptonic meson decays, the hadronic matrix elements are described by the corresponding form factors. We distinguish two scenarios depending on the nature of the outgoing meson. If it is a pseudoscalar (of mass m and momentum p'), the non-vanishing matrix elements are:

$$\begin{aligned}\langle P'(p') | \bar{q}_i \gamma^\mu q_j | P(p) \rangle &= f_+(q^2) \left[(p + p')^\mu - \frac{m_P^2 - m^2}{q^2} q^\mu \right] + f_0(q^2) \frac{m_P^2 - m^2}{q^2} q^\mu, \\ \langle P'(p') | \bar{q}_i q_j | P(p) \rangle &= f_S(q^2), \\ \langle P'(p') | \bar{q}_i \sigma^{\mu\nu} q_j | P(p) \rangle &= \frac{2i}{m_P + m} [p^\mu p'^\nu - p^\nu p'^\mu] f_T(q^2),\end{aligned}\tag{A.2}$$

where $q^\mu \equiv p^\mu - p'^\mu$. Of the four form factors (f_+ , f_0 , f_S and f_T), the scalar one can be related to the others using the equations of motion, through

$$f_S(q^2) = \frac{m_P^2 - m^2}{m_{q_j} - m_{q_i}} f_0(q^2).\tag{A.3}$$

When the final meson is a vector (of mass m , outgoing momentum p' and polarization vector ϵ), the non-zero matrix elements are:

$$\begin{aligned}\langle V(p', \epsilon) | \bar{q}_i \gamma^\mu q_j | P(p) \rangle &= i g(q^2) \epsilon^{\mu\nu\alpha\beta} \epsilon_\nu^* P_\alpha q_\beta, \\ \langle V(p', \epsilon) | \bar{q}_i \gamma^\mu \gamma_5 q_j | P(p) \rangle &= f(q^2) \epsilon^{*\mu} + a_+(q^2) P^\mu \epsilon^* \cdot p + a_-(q^2) q^\mu \epsilon^* \cdot p, \\ \langle V(p', \epsilon) | \bar{q}_i \sigma^{\mu\nu} q_j | P(p) \rangle &= \epsilon^{\mu\nu\alpha\beta} (g_+(q^2) \epsilon_\alpha^* P_\beta + g_-(q^2) \epsilon_\alpha^* q_\beta + g_0(q^2) p_\alpha p'_\beta \epsilon^* \cdot p), \\ \langle V(p', \epsilon) | \bar{q}_i \gamma_5 q_j | P(p) \rangle &= f_{PS}(q^2) \epsilon^* \cdot p,\end{aligned}\tag{A.4}$$

where we defined $P^\mu \equiv p^\mu + p'^\mu$. These transitions, denoted by $P \rightarrow V$, are parametrized by eight functions of q^2 : g , f , a_+ , a_- , g_+ , g_- , g_0 and f_{PS} . Equations of motion relate the pseudoscalar form factor with the rest through the following expression:

$$f_{PS}(q^2) = \frac{1}{m_{q_i} + m_{q_j}} [f(q^2) + a_+(q^2) (m_P^2 - m^2) + a_-(q^2) q^2].\tag{A.5}$$

A.1 Two-body decays

In the rest frame of a particle of mass M , the two-body decay width reads

$$\Gamma = \frac{\lambda^{1/2}(M^2, m_a^2, m_b^2)}{64\pi^2 M^3} \int d\Omega_{\text{cm}} \sum_{\text{spins}} |\mathcal{M}|^2,\tag{A.6}$$

where $\lambda(x, y, z) \equiv (x - y - z)^2 - 4yz$, and m_a, m_b denote the masses of the decay products. Note that for identical particles in the final state one has $\int d\Omega_{\text{cm}} = 2\pi$.

In this section, we list the amplitudes and corresponding partial decay widths of a neutral pseudoscalar meson $P \sim \bar{q}_i q_j$ decaying into (i) a pair of HNLs, and (ii) one HNL plus one active neutrino. For a Dirac HNL (and Dirac ν), these decays occur via the LNC pair- N_R operators in table 1 and the LNC single- N_R operators in table 2. In the Majorana scenario (where the HNL and ν are Majorana), the decays receive contributions from both the LNC and LNV operators. The amplitudes for Dirac neutrinos read

$$\mathcal{M}(P \rightarrow N\bar{N}) = i \frac{f_P}{2} \left(c_{qN,ij}^{V,RR} - c_{qN,ij}^{V,LR} \right) \bar{u}_N \not{P} P_R v_{N'}, \quad (\text{A.7})$$

$$\mathcal{M}(P \rightarrow \nu_\alpha \bar{N}) = i \frac{f_P^S}{2} \left(c_{q\nu N,ij\alpha}^{S,RR} - c_{q\nu N,ij\alpha}^{S,LR} \right) \bar{u}_\nu P_R v_N, \quad (\text{A.8})$$

where u_N (u_ν) and v_N are the spinors corresponding to N (ν) and \bar{N} , respectively. A prime is added when there are two HNLs in the final state. For Majorana neutrinos, we recall that the full Majorana HNL field is $N = N_R^c + N_R$, such that $N^c = N$. The amplitude for $P \rightarrow NN$ has to be anti-symmetrized in N and N' , since there are two identical particles in the final state.¹²

$$\begin{aligned} \mathcal{M}(P \rightarrow NN) &= i \frac{f_P}{2} \left(c_{qN,ij}^{V,RR} - c_{qN,ij}^{V,LR} \right) \bar{u}_N \not{P} \gamma_5 v_{N'} \\ &\quad + i f_P^S \left[\left(c_{qN,ij}^{S,RR} - c_{qN,ij}^{S,LR} \right) \bar{u}_N P_R v_{N'} - \left(c_{qN,ji}^{S,RR*} - c_{qN,ji}^{S,LR*} \right) \bar{u}_N P_L v_{N'} \right], \quad (\text{A.9}) \\ \mathcal{M}(P \rightarrow \nu_\alpha N) &= i \frac{f_P^S}{2} \left[\left(c_{q\nu N,ij\alpha}^{S,RR} - c_{q\nu N,ij\alpha}^{S,LR} \right) \bar{u}_\nu P_R v_N - \left(c_{q\nu N,ji\alpha}^{S,RR*} - c_{q\nu N,ji\alpha}^{S,LR*} \right) \bar{u}_\nu P_L v_N \right] \\ &\quad + i \frac{f_P}{2} \left[\left(c_{q\nu N,ij\alpha}^{V,RR} - c_{q\nu N,ij\alpha}^{V,LR} \right) \bar{u}_\nu \not{P} P_R v_N - \left(c_{q\nu N,ji\alpha}^{V,RR*} - c_{q\nu N,ji\alpha}^{V,LR*} \right) \bar{u}_\nu \not{P} P_L v_N \right]. \quad (\text{A.10}) \end{aligned}$$

The decay rates of these two processes in the Dirac scenario are given by

$$\Gamma(P \rightarrow N\bar{N}) = \frac{|f_P|^2}{32\pi} \left| c_{qN,ij}^{V,RR} - c_{qN,ij}^{V,LR} \right|^2 m_P m_N^2 \sqrt{1 - \frac{4m_N^2}{m_P^2}}, \quad (\text{A.11})$$

$$\Gamma(P \rightarrow \nu_\alpha \bar{N}) = \frac{|f_P^S|^2}{64\pi} \left| c_{q\nu N,ij\alpha}^{S,RR} - c_{q\nu N,ij\alpha}^{S,LR} \right|^2 m_P \left(1 - \frac{m_N^2}{m_P^2} \right)^2, \quad (\text{A.12})$$

and in the Majorana case by

$$\Gamma(P \rightarrow NN) = \frac{m_P}{32\pi} \sqrt{1 - \frac{4m_N^2}{m_P^2}} \left[2|f_P|^2 \left| c_{qN,ij}^{V,RR} - c_{qN,ij}^{V,LR} \right|^2 m_N^2 \right.$$

¹²The convention for associating a u or v spinor to a Majorana particle is arbitrary. Our is such that there is one \bar{u} spinor and one v spinor in each process. In this way, we recover the usual Dirac relations for the sums over spins. Nonetheless, the physical result does not depend on the convention's choice.

$$\begin{aligned}
& + |f_P^S|^2 \left\{ \left(|c_{qN,ij}^{S,RR} - c_{qN,ij}^{S,LR}|^2 + |c_{qN,ji}^{S,RR} - c_{qN,ji}^{S,LR}|^2 \right) \left(1 - \frac{2m_N^2}{m_P^2} \right) \right. \\
& \quad \left. + 2 \left[\left(c_{qN,ij}^{S,RR} - c_{qN,ij}^{S,LR} \right) \left(c_{qN,ji}^{S,RR} - c_{qN,ji}^{S,LR} \right) + \text{h.c.} \right] \frac{m_N^2}{m_P^2} \right\} \\
& + f_P f_P^S \left\{ \left(c_{qN,ij}^{V,RR} - c_{qN,ij}^{V,LR} \right) \left(c_{qN,ij}^{S,RR*} - c_{qN,ij}^{S,LR*} + c_{qN,ji}^{S,RR} - c_{qN,ji}^{S,LR} \right) m_N + \text{h.c.} \right\} \Bigg], \\
\end{aligned} \tag{A.13}$$

$$\begin{aligned}
\Gamma(P \rightarrow \nu_\alpha N) &= \frac{m_P}{64\pi} \left(1 - \frac{m_N^2}{m_P^2} \right)^2 \left[|f_P^S|^2 \left(|c_{q\nu N,ij\alpha}^{S,RR} - c_{q\nu N,ij\alpha}^{S,LR}|^2 + |c_{q\nu N,ji\alpha}^{S,RR} - c_{q\nu N,ji\alpha}^{S,LR}|^2 \right) \right. \\
& + |f_P|^2 \left(|c_{q\nu N,ij\alpha}^{V,RR} - c_{q\nu N,ij\alpha}^{V,LR}|^2 + |c_{q\nu N,ji\alpha}^{V,RR} - c_{q\nu N,ji\alpha}^{V,LR}|^2 \right) m_N^2 \\
& + f_P f_P^S \left\{ \left[\left(c_{q\nu N,ij\alpha}^{S,RR} - c_{q\nu N,ij\alpha}^{S,LR} \right) \left(c_{q\nu N,ji\alpha}^{V,RR} - c_{q\nu N,ji\alpha}^{V,LR} \right) \right. \right. \\
& \quad \left. \left. + \left(c_{q\nu N,ji\alpha}^{S,RR*} - c_{q\nu N,ji\alpha}^{S,LR*} \right) \left(c_{q\nu N,ij\alpha}^{V,RR*} - c_{q\nu N,ij\alpha}^{V,LR*} \right) \right] m_N + \text{h.c.} \right\} \Bigg]. \\
\end{aligned} \tag{A.14}$$

A.2 Three-body decays

For the three-body phase space integral calculations we follow the procedure described in Ref. [17, Appendix B.1]. However, we adopt general labels for the leptonic products. In the rest frame of the decaying pseudoscalar meson, the decay rate reads

$$\begin{aligned}
\Gamma &= \frac{1}{2m_P} \frac{1}{(2\pi)^5} \int d^4 p' \int d^4 p_a \int d^4 p_b \delta(p'^2 - m^2) \delta(p_a^2 - m_a^2) \delta(p_b^2 - m_b^2) \\
& \times \sum_{\text{spins}} |\mathcal{M}|^2 \delta^{(4)}(p - p' - p_a - p_b), \\
\end{aligned} \tag{A.15}$$

where p (p') is the momentum of the decaying (outgoing) meson and p_a and p_b denote the momenta of the produced leptons.¹³ The summed over spins squared matrix element can be written in terms of four-momentum invariant scalar products and the hadronic form factors, which are functions of $q^2 = (p - p')^2$. After performing the integral over the four-momentum p_b , it is convenient to introduce the variable a via a factor of $1 = \int da \delta(a - q^2)$. Then, the spin-summed matrix element squared can be written as

$$\sum_{\text{spins}} |\mathcal{M}|^2 \Big|_{p_b=q-p_a} = \sum_{n=0}^K c_n(a) (p_a \cdot p)^n, \tag{A.16}$$

where $c_n(a)$ are functions of a , particle masses and the hadronic form factors. For the decays under study we have $K \leq 2$. After performing the remaining momentum integrals,

¹³The labels a and b will refer to (i) N' and N , and (ii) ν and N .

one arrives at the final decay rate expression¹⁴

$$\Gamma = \frac{1}{2m_P} \frac{1}{(2\pi)^5} \int_{(m_a+m_b)^2}^{(m_P-m)^2} da I_P \sum_{n=0}^K c_n(a) I_n, \quad (\text{A.17})$$

where the integrals I_P and I_n (for $n = 0, 1, 2$) are given by

$$\begin{aligned} I_P &= \frac{\pi}{2m_P^2} \lambda^{1/2}(a, m^2, m_P^2), \\ I_0 &= \frac{\pi}{2a} \lambda^{1/2}(a, m_a^2, m_b^2), \quad I_1 = \frac{(p_a \cdot q)(p \cdot q)}{a} I_0, \\ I_2 &= \frac{I_0}{a^2} \left((p_a \cdot q)^2 (p \cdot q)^2 + \frac{1}{48} \lambda(a, m^2, m_P^2) \lambda(a, m_a^2, m_b^2) \right). \end{aligned} \quad (\text{A.18})$$

The scalar products above have to be replaced by

$$p_a \cdot q = \frac{1}{2} (a + m_a^2 - m_b^2), \quad p \cdot q = \frac{1}{2} (m_P^2 + a - m^2). \quad (\text{A.19})$$

In summary, after computing the spin-summed matrix element squared with standard techniques and arranging it in the form of Eq. (A.16), one replaces $(p_a \cdot p)^n$ by the corresponding integral result I_n , substitutes the form factor expressions (see section A.3), and evaluates the integral in Eq. (A.17) numerically.

In the rest of this section, we give the amplitudes of the relevant three-body decays for producing the HNLs via the N_R LEFT operators. For Dirac HNLs, these are

$$\mathcal{M}(P \rightarrow P' N \bar{N}) = \frac{1}{2} \left(c_{qN,ij}^{V,RR} + c_{qN,ij}^{V,LR} \right) \left(f_+ P_\mu + (f_0 - f_+) \frac{m_P^2 - m^2}{q^2} q_\mu \right) [\bar{u}_N \gamma^\mu P_R v_{N'}], \quad (\text{A.20})$$

$$\begin{aligned} \mathcal{M}(P \rightarrow V N \bar{N}) &= \left\{ \left(c_{qN,ij}^{V,RR} + c_{qN,ij}^{V,LR} \right) \left(i g \epsilon_{\mu\nu\alpha\beta} \epsilon^{*\nu} p'^\alpha p^\beta \right) \right. \\ &\quad \left. + \frac{1}{2} \left(c_{qN,ij}^{V,RR} - c_{qN,ij}^{V,LR} \right) \left(f \epsilon_\mu^* + a_+ P_\mu \epsilon^* \cdot p + a_- q_\mu \epsilon^* \cdot p \right) \right\} [\bar{u}_N \gamma^\mu P_R v_N], \end{aligned} \quad (\text{A.21})$$

$$\begin{aligned} \mathcal{M}(P \rightarrow P' \nu_\alpha \bar{N}) &= \frac{f_S}{2} \left(c_{q\nu N,ij\alpha}^{S,RR} + c_{q\nu N,ij\alpha}^{S,LR} \right) [\bar{u}_\nu P_R v_N] \\ &\quad + c_{q\nu N,ij\alpha}^{T,RR} \frac{2i f_T}{m_P + m} \left(p_\mu p'_\nu + \frac{i}{2} \epsilon_{\mu\nu\rho\sigma} p^\rho p'^\sigma \right) [\bar{u}_\nu \sigma^{\mu\nu} P_R v_N], \end{aligned} \quad (\text{A.22})$$

$$\begin{aligned} \mathcal{M}(P \rightarrow V \nu_\alpha \bar{N}) &= \frac{f_{PS}}{2} \left(c_{q\nu N,ij\alpha}^{S,RR} - c_{q\nu N,ij\alpha}^{S,LR} \right) (\epsilon^* \cdot p) [\bar{u}_\nu P_R v_N] \\ &\quad + c_{q\nu N,ij\alpha}^{T,RR} \left\{ \frac{1}{2} \epsilon_{\mu\nu\alpha\beta} \left[g_+ \epsilon^{*\alpha} (p + p')^\beta + g_- \epsilon^{*\alpha} q^\beta + g_0 p^\alpha p'^\beta \epsilon^* \cdot p \right] \right. \\ &\quad \left. - i \left[g_+ \epsilon_\mu^* (p + p')_\nu + g_- \epsilon_\mu^* q_\nu + g_0 p_\mu p'_\nu \epsilon^* \cdot p \right] \right\} [\bar{u}_\nu \sigma^{\mu\nu} P_R v_N]. \end{aligned} \quad (\text{A.23})$$

¹⁴When the outgoing leptons are two Majorana HNLs an extra factor of 1/2 appears in the final expression.

The corresponding amplitudes for Majorana HNLs read

$$\begin{aligned}\mathcal{M}(P \rightarrow P' NN) &= \frac{1}{2} \left(c_{qN,ij}^{V,RR} + c_{qN,ij}^{V,LR} \right) \left(f_+ P_\mu + (f_0 - f_+) \frac{m_P^2 - m^2}{q^2} q_\mu \right) [\overline{u_N} \gamma^\mu \gamma^5 v_{N'}] \\ &+ f_S \left(c_{qN,ij}^{S,RR} + c_{qN,ij}^{S,LR} \right) [\overline{u_N} P_R v_{N'}] + f_S \left(c_{qN,ji}^{S,RR*} + c_{qN,ji}^{S,LR*} \right) [\overline{u_N} P_L v_{N'}] ,\end{aligned}\tag{A.24}$$

$$\begin{aligned}\mathcal{M}(P \rightarrow V NN) &= \left\{ \left(c_{qN,ij}^{V,RR} + c_{qN,ij}^{V,LR} \right) \left(i g \epsilon_{\mu\nu\alpha\beta} \epsilon^{*\nu} p'^\alpha p^\beta \right) \right. \\ &+ \frac{1}{2} \left(c_{qN,ij}^{V,RR} - c_{qN,ij}^{V,LR} \right) \left(f \epsilon_\mu^* + a_+ P_\mu \epsilon^* \cdot p + a_- q_\mu \epsilon^* \cdot p \right) \left. \right\} [\overline{u_N} \gamma^\mu \gamma^5 v_{N'}] \\ &+ f_{PS} \left\{ \left(c_{q\nu N,ij}^{S,RR} - c_{q\nu N,ij}^{S,LR} \right) (\epsilon^* \cdot p) [\overline{u_N} P_R v_{N'}] \right. \\ &\quad \left. - \left(c_{q\nu N,ji}^{S,RR*} - c_{q\nu N,ji}^{S,LR*} \right) (\epsilon^* \cdot p) [\overline{u_N} P_L v_{N'}] \right\} ,\end{aligned}\tag{A.25}$$

$$\begin{aligned}\mathcal{M}(P \rightarrow P' \nu_\alpha N) &= \frac{f_S}{2} \left\{ \left(c_{q\nu N,ij\alpha}^{S,RR} + c_{q\nu N,ij\alpha}^{S,LR} \right) [\overline{u_\nu} P_R v_N] + \left(c_{q\nu N,ji\alpha}^{S,RR*} + c_{q\nu N,ji\alpha}^{S,LR*} \right) [\overline{u_\nu} P_L v_N] \right\} \\ &+ \frac{if_T}{M+m} \left\{ c_{q\nu N,ij\alpha}^{T,RR} (2p_\mu p'_\nu + i \epsilon_{\mu\nu\rho\sigma} p^\rho p'^\sigma) [\overline{u_\nu} \sigma^{\mu\nu} P_R v_N] \right. \\ &\quad \left. - c_{q\nu N,ji\alpha}^{T,RR*} (2p_\mu p'_\nu - i \epsilon_{\mu\nu\rho\sigma} p^\rho p'^\sigma) [\overline{u_\nu} \sigma^{\mu\nu} P_L v_N] \right\} \\ &+ \left\{ \left(c_{q\nu N,ij\alpha}^{V,RR} + c_{q\nu N,ij\alpha}^{V,LR} \right) [\overline{u_\nu} \gamma^\mu P_R v_N] - \left(c_{q\nu N,ji\alpha}^{V,RR*} + c_{q\nu N,ji\alpha}^{V,LR*} \right) [\overline{u_\nu} \gamma^\mu P_L v_N] \right\} \\ &\times \frac{1}{2} \left(f_+ P_\mu + (f_0 - f_+) \frac{m_P^2 - m^2}{q^2} q_\mu \right) ,\end{aligned}\tag{A.26}$$

$$\begin{aligned}\mathcal{M}(P \rightarrow V \nu_\alpha N) &= \frac{f_{PS}}{2} \left\{ \left(c_{q\nu N,ij\alpha}^{S,RR} - c_{q\nu N,ij\alpha}^{S,LR} \right) (\epsilon^* \cdot p) [\overline{u_\nu} P_R v_N] \right. \\ &\quad \left. - \left(c_{q\nu N,ji\alpha}^{S,RR*} - c_{q\nu N,ji\alpha}^{S,LR*} \right) (\epsilon^* \cdot p) [\overline{u_\nu} P_L v_N] \right\} \\ &+ c_{q\nu N,ij\alpha}^{T,RR} \left(\frac{1}{2} \epsilon_{\mu\nu\alpha\beta} T^{\alpha\beta} - iT_{\mu\nu} \right) [\overline{u_\nu} \sigma^{\mu\nu} P_R v_N] \\ &- c_{q\nu N,ji\alpha}^{T,RR*} \left(\frac{1}{2} \epsilon_{\mu\nu\alpha\beta} T^{\alpha\beta} + iT_{\mu\nu} \right) [\overline{u_\nu} \sigma^{\mu\nu} P_L v_N] \\ &+ \frac{1}{2} \left\{ \left(c_{q\nu N,ij\alpha}^{V,RR} + c_{q\nu N,ij\alpha}^{V,LR} \right) V_\mu + \left(c_{q\nu N,ij\alpha}^{V,RR} - c_{q\nu N,ij\alpha}^{V,LR} \right) A_\mu \right\} [\overline{u_\nu} \gamma^\mu P_R v_N] \\ &- \frac{1}{2} \left\{ \left(c_{q\nu N,ji\alpha}^{V,RR*} + c_{q\nu N,ji\alpha}^{V,LR*} \right) V_\mu + \left(c_{q\nu N,ji\alpha}^{V,RR*} - c_{q\nu N,ji\alpha}^{V,LR*} \right) A_\mu \right\} [\overline{u_\nu} \gamma^\mu P_L v_N] ,\end{aligned}\tag{A.27}$$

where we have introduced:

$$T^{\alpha\beta} \equiv g_+ \epsilon^{*\alpha} (p + p')^\beta + g_- \epsilon^{*\alpha} q^\beta + g_0 p^\alpha p'^\beta (\epsilon^* \cdot p) ,$$

Meson P	Decay constant f_P [MeV]
D^0	212.0 (0.7)
B^0	190.0 (1.3)
B_s^0	230.3 (1.3)

Table 7. Decay constants of heavy neutral pseudoscalar mesons [75].

$$\begin{aligned}
V_\mu &\equiv 2ig\epsilon_{\mu\nu\alpha\beta}\epsilon^{*\nu}p'^\alpha p^\beta, \\
A_\mu &\equiv f\epsilon_\mu^* + a_+(p+p')_\mu(\epsilon^* \cdot p) + a_-q_\mu(\epsilon^* \cdot p).
\end{aligned}$$

Specific software, such as `FeynCalc` [73, 74], automatizes the computation of the summed over spins squared matrix elements. Finally, to simplify notation in the previous expressions, we have omitted the q^2 dependence of the form factors.

A.3 Decay constants and form factors

The masses of all mesons involved in the decays are taken from Ref. [58]. In addition, we use the light quark masses at a renormalization scale of $\mu = 2$ GeV in $\overline{\text{MS}}$, whereas for m_c and m_b we employ the $\overline{\text{MS}}$ masses at $\mu = m_c$ and $\mu = m_b$, respectively, as in Ref. [58]:

$$m_u = 2.2 \text{ MeV}, \quad m_d = 4.7 \text{ MeV}, \quad m_s = 93 \text{ MeV}, \quad m_c = 1.27 \text{ GeV}, \quad m_b = 4.18 \text{ GeV}.$$

We provide the decay constants of the heavy neutral pseudoscalar mesons in table 7. We use the isospin-averaged results¹⁵ for $N_f = 2 + 1 + 1$ dynamical quark flavors from Ref. [75]. As regards hadronic form factors, several parametrizations exist in the literature for describing their dependence on q^2 . One of the most used is the BCL method [77], and we try to stick to it as long as there is available data. In all other cases, we use the so-called double-pole parametrization. In table 8, we show all hadronic transitions mediated by the selected $N_R\text{LEFT}$ operators and the references studying the associated form factors. We indicate the equation where the explicit q^2 parametrization appears and the tables where the best-fit parameter values are given.¹⁶

B Branching ratios of meson decays triggered by single- N_R operators

We have also computed the branching ratios for two- and three-body pseudoscalar meson decays including in the final state a SM neutrino and an HNL. These decays are triggered by the single- N_R operators given in table 2. As an example, we show in figure 8 the

¹⁵In other words, we assume the isospin symmetry, *i.e.* the (approximate) symmetry between the u and d quarks. In this limit, the decay constants for D^0 and D^+ are the same, f_D . Similarly, B^0 and B^+ mesons are characterised by one constant, f_B . The difference $|f_{P^+} - f_P|$ is estimated to be $\simeq 0.5$ MeV for both $P = D$ and $P = B$ [75, 76].

¹⁶Notice that there are several conventions in the literature for writing hadronic matrix elements in terms of form factors. The basis presented in Eqs. (A.2) and (A.4) must be converted to the new basis in each reference before using their q^2 parametrization.

Meson transitions		Form factor parametrization	Fitted parameters
<i>D</i> -mesons	$D^0 \rightarrow \pi^0$ $D^+ \rightarrow \pi^+$	BCL [78, Eqs. (A1)–(A2)]	[78, Tab. VI]
	$D^0 \rightarrow \eta, \eta', \rho^0, \omega$ $D^+ \rightarrow \rho^+$ $D_s^+ \rightarrow K^+, K^{*+}$	Double-pole [79, Eq. (63)]	[79, Tab. VI]
	$B^0 \rightarrow \pi^0, K^0$ $B^+ \rightarrow \pi^+, K^+$ $B_s^0 \rightarrow \bar{K}^0$	BCL [75, Eqs. (529)–(530)]	[75, Tabs. 46, 48, 50, 51]
	$B^0 \rightarrow \eta, \eta'$ $B_s^0 \rightarrow \eta, \eta'$	Double-pole [80, Eq. (36)]	[80, Tab. 4]
<i>B</i> -mesons	$B^0 \rightarrow \rho^0, \omega, K^{*0}$ $B^+ \rightarrow \rho^+, K^{*+}$ $B_s^0 \rightarrow \phi, \bar{K}^{*0}$	BCL [81, Eq. (2.16)]	[81, Tab. 14]

Table 8. Relevant meson transitions for the decays studied in section 3. The two last columns show the references to the form factor parametrizations and the best-fit parameter values. Isospin symmetry is assumed so that identical form factors are taken for $P^0 \rightarrow M^0$ and $P^+ \rightarrow M^+$ transitions, where M can be a pseudoscalar or vector meson.

corresponding branching ratios in the case of $b \rightarrow d$ transitions triggered by three single- N_R operators, namely, $\mathcal{O}_{d\nu N,31\alpha}^{S,RR}$, $\mathcal{O}_{d\nu N,31\alpha}^{T,RR}$, and $\mathcal{O}_{d\nu N,31\alpha}^{V,RR}$. The scalar and tensor operators are LNC, whereas the operator of the vector type is LNV.

As can be seen from Eq. (A.14), the tensor operator does not contribute to the two-body decay width. This is why there is no solid blue line in the corresponding plot in figure 8. The tensor form factors for the $B \rightarrow \pi$ transitions have been taken from table 50 in Ref. [75]. For $B^0 \rightarrow \eta, \eta'$ and $B_s^0 \rightarrow \bar{K}^0$, we have used Eq. (27) from Ref. [80], which relates f_T to f_+ and f_0 . Finally, for the $B_{(s)} \rightarrow V$ transitions, we have used the results of Ref. [81]. In table 8 we include these references and the ones for all other form factors.

We note that the branching ratios in figure 8 are very similar to those for the meson decays induced by the single- N_R operators with a charged lepton, which have been studied in detail in Ref. [17], cf. figure 2 therein. Thus, the constraints on the neutral current single- N_R operators from the far detectors are expected to be very similar to those derived in Ref. [17] for the charged current single- N_R operators. For this reason, we do not study the neutral current single- N_R operators in more detail.

C HNL two-body decays via single- N_R operators

Single- N_R operators contribute to both HNL production and decay. In fact, depending on the Wilson coefficient and the value of active-heavy mixing, they can even dominate the HNL decay width. The LNC and LNV operators in table 2 make HNLs undergo two- and three-body semileptonic decays. The dominant channels are two-body decays, mediated

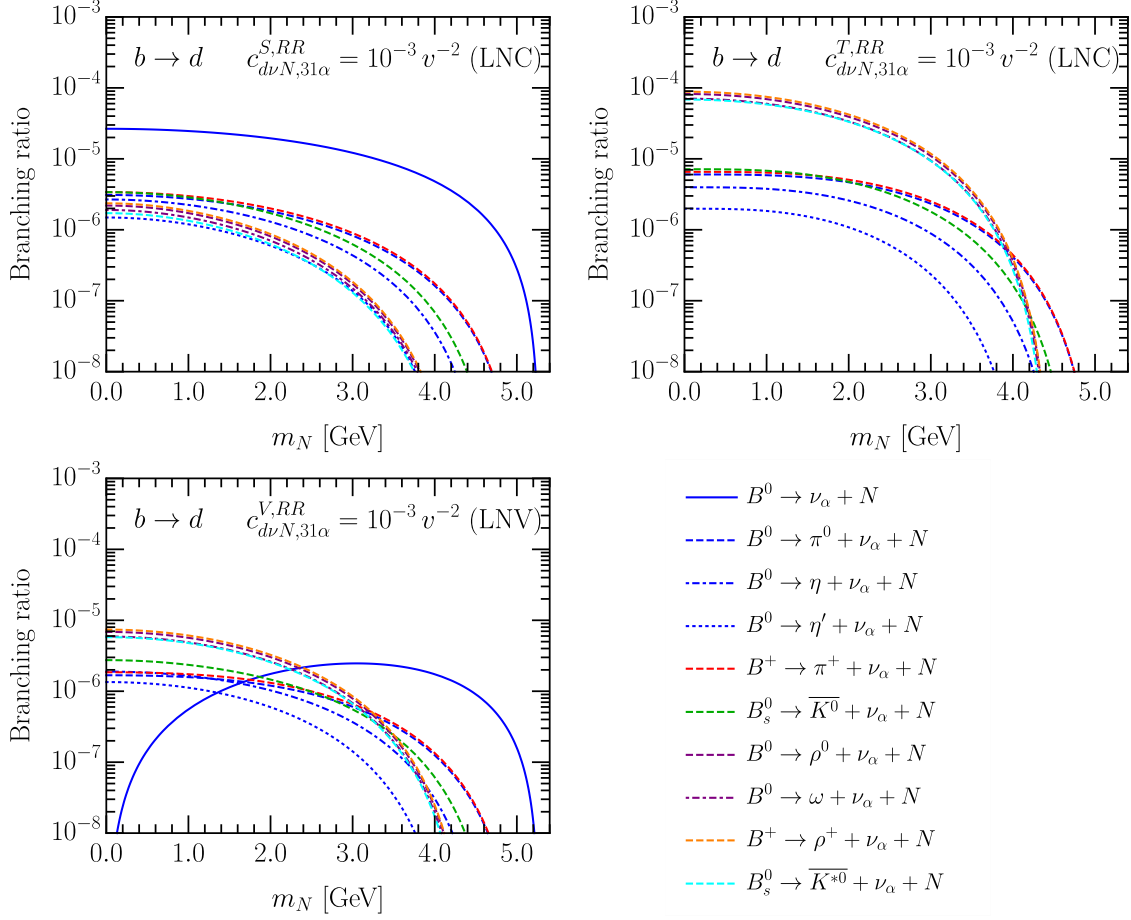


Figure 8. Branching ratios of B -meson decays triggered by the single- N_R operators $\mathcal{O}_{d\nu N,31\alpha}^{S,RR}$, $\mathcal{O}_{d\nu N,31\alpha}^{T,RR}$ and $\mathcal{O}_{d\nu N,32\alpha}^{V,RR}$. In each case, the corresponding Wilson coefficient has been set to $10^{-3}v^{-2}$.

by just one insertion of an effective operator, with one light neutral meson and one active neutrino in the final state. If the HNL mass is large enough, then multimeson final states could also be important in the computation of the total decay width. We do not compute this contribution, though. The single- N_R operators with light quarks can mediate the two-body decay processes mentioned above at tree level. The contribution from operators with heavy quarks, which control B - and D -meson decays into HNLs, is loop-suppressed, and we do not compute it. The interference between active-heavy mixing and single- N_R operators is also not treated here.

In this appendix, we list the HNL partial decay rates into a neutral meson and a SM neutrino mediated by the effective operators containing two light quarks. We leave, however, the flavor indices of the Wilson coefficients unspecified. We consider the scenarios where both N and ν are either Dirac or Majorana particles. In each case, we distinguish between a pseudoscalar and a vector meson in the final state. The latter requires the

introduction of the following form factors:

$$\begin{aligned}\langle 0 | \bar{q}_i \gamma^\mu q_j | V(p, \epsilon) \rangle &= i f_V m_V \epsilon^\mu, \\ \langle 0 | \bar{q}_i \sigma^{\mu\nu} q_j | V(p, \epsilon) \rangle &= -f_V^T (p^\mu \epsilon^\nu - p^\nu \epsilon^\mu),\end{aligned}\quad (\text{C.1})$$

where $|V(p, \epsilon)\rangle$ denotes a vector meson with mass m_V , momentum p , and polarization vector ϵ . For Dirac N and ν , the decay rate into a SM neutrino and a pseudoscalar (vector) meson P (V) $\sim \bar{q}_i q_j$ of mass m_P (m_V) reads

$$\Gamma(N \rightarrow \nu_\alpha P) = \frac{|f_P^S|^2}{128\pi} \left| c_{q\nu N, ji\alpha}^{S,RR} - c_{q\nu N, ji\alpha}^{S,LR} \right|^2 m_N \left(1 - \frac{m_P^2}{m_N^2} \right)^2, \quad (\text{C.2})$$

$$\Gamma(N \rightarrow \nu_\alpha V) = \frac{|f_V^T|^2}{4\pi} \left| c_{q\nu N, ji\alpha}^{T,RR} \right|^2 m_N^3 \left(1 - \frac{m_V^2}{m_N^2} \right)^2 \left(1 + \frac{m_V^2}{2m_N^2} \right). \quad (\text{C.3})$$

In the Majorana scenario, the decay rates receive contributions from both the LNC and LNV single- N_R operators and are given by

$$\begin{aligned}\Gamma(N \rightarrow \nu_\alpha P) &= \frac{m_N}{128\pi} \left(1 - \frac{m_P^2}{m_N^2} \right)^2 \left\{ |f_P^S|^2 \left(\left| c_{q\nu N, ji\alpha}^{S,RR} - c_{q\nu N, ji\alpha}^{S,LR} \right|^2 + \left| c_{q\nu N, ij\alpha}^{S,RR} - c_{q\nu N, ij\alpha}^{S,LR} \right|^2 \right) \right. \\ &\quad + |f_P|^2 \left(\left| c_{q\nu N, ji\alpha}^{V,RR} - c_{q\nu N, ji\alpha}^{V,LR} \right|^2 + \left| c_{q\nu N, ij\alpha}^{V,RR} - c_{q\nu N, ij\alpha}^{V,LR} \right|^2 \right) m_N^2 \\ &\quad - f_P f_P^S \left[\left(c_{q\nu N, ji\alpha}^{S,RR} - c_{q\nu N, ji\alpha}^{S,LR} \right) \left(c_{q\nu N, ij\alpha}^{V,RR} - c_{q\nu N, ij\alpha}^{V,LR} \right) \right. \\ &\quad \left. \left. + \left(c_{q\nu N, ij\alpha}^{S,RR} - c_{q\nu N, ij\alpha}^{S,LR} \right) \left(c_{q\nu N, ji\alpha}^{V,RR} - c_{q\nu N, ji\alpha}^{V,LR} \right) + \text{h.c.} \right] m_N \right\}, \quad (\text{C.4})\end{aligned}$$

$$\begin{aligned}\Gamma(N \rightarrow \nu_\alpha V) &= \frac{m_N^3}{128\pi} \left(1 - \frac{m_V^2}{m_N^2} \right)^2 \left\{ 32 |f_V^T|^2 \left(\left| c_{q\nu N, ij\alpha}^{T,RR} \right|^2 + \left| c_{q\nu N, ji\alpha}^{T,RR} \right|^2 \right) \left(1 + \frac{m_V^2}{2m_N^2} \right) \right. \\ &\quad + |f_V|^2 \left(\left| c_{q\nu N, ji\alpha}^{V,RR} + c_{q\nu N, ji\alpha}^{V,LR} \right|^2 + \left| c_{q\nu N, ij\alpha}^{V,RR} + c_{q\nu N, ij\alpha}^{V,LR} \right|^2 \right) \left(1 + \frac{2m_V^2}{m_N^2} \right) \\ &\quad - 12 f_V^T f_V \left[c_{q\nu N, ji\alpha}^{T,RR} \left(c_{q\nu N, ij\alpha}^{V,RR} + c_{q\nu N, ij\alpha}^{V,LR} \right) \right. \\ &\quad \left. \left. + c_{q\nu N, ij\alpha}^{T,RR} \left(c_{q\nu N, ji\alpha}^{V,RR} + c_{q\nu N, ji\alpha}^{V,LR} \right) + \text{h.c.} \right] \frac{m_V}{m_N} \right\}. \quad (\text{C.5})\end{aligned}$$

References

- [1] J. Alimena et al., *Searching for long-lived particles beyond the Standard Model at the Large Hadron Collider*, *J. Phys. G* **47** (2020) 090501 [[1903.04497](#)].
- [2] D. Curtin et al., *Long-Lived Particles at the Energy Frontier: The MATHUSLA Physics Case*, *Rept. Prog. Phys.* **82** (2019) 116201 [[1806.07396](#)].
- [3] M. Bauer, O. Brandt, L. Lee and C. Ohm, *ANUBIS: Proposal to search for long-lived neutral particles in CERN service shafts*, [1909.13022](#).

- [4] V.V. Gligorov, S. Knapen, B. Nachman, M. Papucci and D.J. Robinson, *Leveraging the ALICE/L3 cavern for long-lived particle searches*, *Phys. Rev. D* **99** (2019) 015023 [[1810.03636](#)].
- [5] V.V. Gligorov, S. Knapen, M. Papucci and D.J. Robinson, *Searching for Long-lived Particles: A Compact Detector for Exotics at LHCb*, *Phys. Rev. D* **97** (2018) 015023 [[1708.09395](#)].
- [6] S. Cerci et al., *FACET: A new long-lived particle detector in the very forward region of the CMS experiment*, *JHEP* **2022** (2022) 110 [[2201.00019](#)].
- [7] J.L. Feng, I. Galon, F. Kling and S. Trojanowski, *ForwArd Search ExpeRiment at the LHC*, *Phys. Rev. D* **97** (2018) 035001 [[1708.09389](#)].
- [8] FASER collaboration, *FASER’s physics reach for long-lived particles*, *Phys. Rev. D* **99** (2019) 095011 [[1811.12522](#)].
- [9] J.L. Pinfold, *The MoEDAL Experiment at the LHC—A Progress Report*, *Universe* **5** (2019) 47.
- [10] J.L. Pinfold, *The MoEDAL experiment: a new light on the high-energy frontier*, *Phil. Trans. Roy. Soc. Lond. A* **377** (2019) 20190382.
- [11] J.P. Chou, D. Curtin and H.J. Lubatti, *New Detectors to Explore the Lifetime Frontier*, *Phys. Lett. B* **767** (2017) 29 [[1606.06298](#)].
- [12] MATHUSLA collaboration, *An Update to the Letter of Intent for MATHUSLA: Search for Long-Lived Particles at the HL-LHC*, [2009.01693](#).
- [13] F. Kling and S. Trojanowski, *Heavy Neutral Leptons at FASER*, *Phys. Rev. D* **97** (2018) 095016 [[1801.08947](#)].
- [14] J.C. Helo, M. Hirsch and Z.S. Wang, *Heavy neutral fermions at the high-luminosity LHC*, *JHEP* **07** (2018) 056 [[1803.02212](#)].
- [15] D. Dercks, H.K. Dreiner, M. Hirsch and Z.S. Wang, *Long-Lived Fermions at AL3X*, *Phys. Rev. D* **99** (2019) 055020 [[1811.01995](#)].
- [16] M. Hirsch and Z.S. Wang, *Heavy neutral leptons at ANUBIS*, *Phys. Rev. D* **101** (2020) 055034 [[2001.04750](#)].
- [17] J. De Vries, H.K. Dreiner, J.Y. Günther, Z.S. Wang and G. Zhou, *Long-lived Sterile Neutrinos at the LHC in Effective Field Theory*, *JHEP* **03** (2021) 148 [[2010.07305](#)].
- [18] M. Ovchinnikov, V. Kryshnal and K. Bondarenko, *Sensitivity of the FACET experiment to Heavy Neutral Leptons and Dark Scalars*, [2209.14870](#).
- [19] G. Cottin, J.C. Helo and M. Hirsch, *Searches for light sterile neutrinos with multitrack displaced vertices*, *Phys. Rev. D* **97** (2018) 055025 [[1801.02734](#)].
- [20] G. Cottin, J.C. Helo and M. Hirsch, *Displaced vertices as probes of sterile neutrino mixing at the LHC*, *Phys. Rev. D* **98** (2018) 035012 [[1806.05191](#)].
- [21] K. Cheung, Y.-L. Chung, H. Ishida and C.-T. Lu, *Sensitivity reach on heavy neutral leptons and τ -neutrino mixing $|U_{\tau N}|^2$ at the HL-LHC*, *Phys. Rev. D* **102** (2020) 075038 [[2004.11537](#)].
- [22] J. Jones-Pérez, J. Masias and J.D. Ruiz-Álvarez, *Search for Long-Lived Heavy Neutrinos at the LHC with a VBF Trigger*, *Eur. Phys. J. C* **80** (2020) 642 [[1912.08206](#)].

- [23] J. Liu, Z. Liu, L.-T. Wang and X.-P. Wang, *Seeking for sterile neutrinos with displaced leptons at the LHC*, *JHEP* **07** (2019) 159 [[1904.01020](#)].
- [24] ATLAS collaboration, *Search for heavy neutral leptons in decays of W bosons produced in 13 TeV pp collisions using prompt and displaced signatures with the ATLAS detector*, *JHEP* **10** (2019) 265 [[1905.09787](#)].
- [25] CMS collaboration, *Search for long-lived heavy neutral leptons with displaced vertices in proton-proton collisions at $\sqrt{s}=13$ TeV*, [2201.05578](#).
- [26] C.-W. Chiang, G. Cottin, A. Das and S. Mandal, *Displaced heavy neutrinos from Z' decays at the LHC*, *JHEP* **12** (2019) 070 [[1908.09838](#)].
- [27] F. Deppisch, S. Kulkarni and W. Liu, *Heavy neutrino production via Z' at the lifetime frontier*, *Phys. Rev. D* **100** (2019) 035005 [[1905.11889](#)].
- [28] I. Brivio and M. Trott, *The Standard Model as an Effective Field Theory*, *Phys. Rept.* **793** (2019) 1 [[1706.08945](#)].
- [29] F. del Aguila, S. Bar-Shalom, A. Soni and J. Wudka, *Heavy Majorana Neutrinos in the Effective Lagrangian Description: Application to Hadron Colliders*, *Phys. Lett. B* **670** (2009) 399 [[0806.0876](#)].
- [30] A. Aparici, K. Kim, A. Santamaria and J. Wudka, *Right-handed neutrino magnetic moments*, *Phys. Rev. D* **80** (2009) 013010 [[0904.3244](#)].
- [31] Y. Liao and X.-D. Ma, *Operators up to Dimension Seven in Standard Model Effective Field Theory Extended with Sterile Neutrinos*, *Phys. Rev. D* **96** (2017) 015012 [[1612.04527](#)].
- [32] H.-L. Li, Z. Ren, M.-L. Xiao, J.-H. Yu and Y.-H. Zheng, *Operator bases in effective field theories with sterile neutrinos: $d \leq 9$* , *JHEP* **11** (2021) 003 [[2105.09329](#)].
- [33] G. Cottin, J.C. Helo, M. Hirsch, A. Titov and Z.S. Wang, *Heavy neutral leptons in effective field theory and the high-luminosity LHC*, *JHEP* **09** (2021) 039 [[2105.13851](#)].
- [34] R. Beltrán, G. Cottin, J.C. Helo, M. Hirsch, A. Titov and Z.S. Wang, *Long-lived heavy neutral leptons at the LHC: four-fermion single- N_R operators*, *JHEP* **01** (2022) 044 [[2110.15096](#)].
- [35] E.E. Jenkins, A.V. Manohar and P. Stoffer, *Low-Energy Effective Field Theory below the Electroweak Scale: Operators and Matching*, *JHEP* **03** (2018) 016 [[1709.04486](#)].
- [36] I. Bischer and W. Rodejohann, *General neutrino interactions from an effective field theory perspective*, *Nucl. Phys. B* **947** (2019) 114746 [[1905.08699](#)].
- [37] M. Chala and A. Titov, *One-loop matching in the SMEFT extended with a sterile neutrino*, *JHEP* **05** (2020) 139 [[2001.07732](#)].
- [38] T. Li, X.-D. Ma and M.A. Schmidt, *General neutrino interactions with sterile neutrinos in light of coherent neutrino-nucleus scattering and meson invisible decays*, *JHEP* **07** (2020) 152 [[2005.01543](#)].
- [39] T. Li, X.-D. Ma and M.A. Schmidt, *Constraints on the charged currents in general neutrino interactions with sterile neutrinos*, *JHEP* **10** (2020) 115 [[2007.15408](#)].
- [40] G. Zhou, J.Y. Günther, Z.S. Wang, J. de Vries and H.K. Dreiner, *Long-lived sterile neutrinos at Belle II in effective field theory*, *JHEP* **04** (2022) 057 [[2111.04403](#)].

- [41] T. Han, J. Liao, H. Liu and D. Marfatia, *Right-handed Dirac and Majorana neutrinos at Belle II*, [2207.07029](#).
- [42] D. Barducci, E. Bertuzzo, M. Taoso and C. Toni, *Probing right-handed neutrinos dipole operators*, [2209.13469](#).
- [43] R.M. Fonseca, *The Sym2Int program: going from symmetries to interactions*, *J. Phys. Conf. Ser.* **873** (2017) 012045 [[1703.05221](#)].
- [44] R.M. Fonseca, *Enumerating the operators of an effective field theory*, *Phys. Rev. D* **101** (2020) 035040 [[1907.12584](#)].
- [45] W. Dekens, J. de Vries, K. Fuyuto, E. Mereghetti and G. Zhou, *Sterile neutrinos and neutrinoless double beta decay in effective field theory*, *JHEP* **06** (2020) 097 [[2002.07182](#)].
- [46] W. Dekens, J. de Vries and T. Tong, *Sterile neutrinos with non-standard interactions in β - and $0\nu\beta\beta$ -decay experiments*, *JHEP* **08** (2021) 128 [[2104.00140](#)].
- [47] J. de Vries, G. Li, M.J. Ramsey-Musolf and J.C. Vasquez, *Light Sterile Neutrinos, Left-Right Symmetry, and $0\nu\beta\beta$ Decay*, [2209.03031](#).
- [48] V. Cirigliano et al., *Neutrinoless Double-Beta Decay: A Roadmap for Matching Theory to Experiment*, [2203.12169](#).
- [49] S. Bhattacharya and J. Wudka, *Dimension-seven operators in the standard model with right handed neutrinos*, *Phys. Rev. D* **94** (2016) 055022 [[1505.05264](#)].
- [50] E.E. Jenkins, A.V. Manohar and P. Stoffer, *Low-Energy Effective Field Theory below the Electroweak Scale: Anomalous Dimensions*, *JHEP* **01** (2018) 084 [[1711.05270](#)].
- [51] M. Chala and A. Titov, *One-loop running of dimension-six Higgs-neutrino operators and implications of a large neutrino dipole moment*, *JHEP* **09** (2020) 188 [[2006.14596](#)].
- [52] A. Datta, J. Kumar, H. Liu and D. Marfatia, *Anomalous dimensions from gauge couplings in SMEFT with right-handed neutrinos*, *JHEP* **02** (2021) 015 [[2010.12109](#)].
- [53] A. Datta, J. Kumar, H. Liu and D. Marfatia, *Anomalous dimensions from Yukawa couplings in SMNEFT: four-fermion operators*, *JHEP* **05** (2021) 037 [[2103.04441](#)].
- [54] M. Hirsch, H.V. Klapdor-Kleingrothaus and S.G. Kovalenko, *New low-energy leptoquark interactions*, *Phys. Lett. B* **378** (1996) 17 [[hep-ph/9602305](#)].
- [55] K. Bondarenko, A. Boyarsky, D. Gorbunov and O. Ruchayskiy, *Phenomenology of GeV-scale Heavy Neutral Leptons*, *JHEP* **11** (2018) 032 [[1805.08567](#)].
- [56] P. Ballett, T. Boschi and S. Pascoli, *Heavy Neutral Leptons from low-scale seesaws at the DUNE Near Detector*, *JHEP* **03** (2020) 111 [[1905.00284](#)].
- [57] P. Coloma, E. Fernández-Martínez, M. González-López, J. Hernández-García and Z. Pavlovic, *GeV-scale neutrinos: interactions with mesons and DUNE sensitivity*, *Eur. Phys. J. C* **81** (2021) 78 [[2007.03701](#)].
- [58] PARTICLE DATA GROUP collaboration, *Review of Particle Physics*, *PTEP* **2022** (2022) 083C01.
- [59] LHCb collaboration, *Measurement of the B_c^- meson production fraction and asymmetry in 7 and 13 TeV pp collisions*, *Phys. Rev. D* **100** (2019) 112006 [[1910.13404](#)].

- [60] T. Sjöstrand, S. Ask, J.R. Christiansen, R. Corke, N. Desai, P. Ilten et al., *An introduction to PYTHIA 8.2*, *Comput. Phys. Commun.* **191** (2015) 159 [[1410.3012](#)].
- [61] C. Bierlich et al., *A comprehensive guide to the physics and usage of pythia 8.3*, [2203.11601](#).
- [62] “Forward Physics in PYTHIA 8.”
<https://pythia.org/download/talks/SjostrandForward20.pdf>.
- [63] A. Atre, T. Han, S. Pascoli and B. Zhang, *The Search for Heavy Majorana Neutrinos*, *JHEP* **05** (2009) 030 [[0901.3589](#)].
- [64] M. Cacciari, M. Greco and P. Nason, *The $P(T)$ spectrum in heavy flavor hadroproduction*, *JHEP* **05** (1998) 007 [[hep-ph/9803400](#)].
- [65] M. Cacciari, S. Frixione and P. Nason, *The $p(T)$ spectrum in heavy flavor photoproduction*, *JHEP* **03** (2001) 006 [[hep-ph/0102134](#)].
- [66] NA62 collaboration, *Search for heavy neutral lepton production in K^+ decays to positrons*, *Phys. Lett. B* **807** (2020) 135599 [[2005.09575](#)].
- [67] T2K collaboration, *Search for heavy neutrinos with the T2K near detector ND280*, *Phys. Rev. D* **100** (2019) 052006 [[1902.07598](#)].
- [68] CHARM collaboration, *A Search for Decays of Heavy Neutrinos in the Mass Range 0.5-GeV to 2.8-GeV*, *Phys. Lett. B* **166** (1986) 473.
- [69] G. Bernardi et al., *Further Limits On Heavy Neutrino Couplings*, *Phys. Lett. B* **203** (1988) 332.
- [70] S.A. Baranov et al., *Search for heavy neutrinos at the IHEP-JINR neutrino detector*, *Phys. Lett. B* **302** (1993) 336.
- [71] BELLE collaboration, *Search for heavy neutrinos at Belle*, *Phys. Rev. D* **87** (2013) 071102 [[1301.1105](#)].
- [72] DELPHI collaboration, *Search for neutral heavy leptons produced in Z decays*, *Z. Phys. C* **74** (1997) 57.
- [73] V. Shtabovenko, R. Mertig and F. Orellana, *New Developments in FeynCalc 9.0*, *Comput. Phys. Commun.* **207** (2016) 432 [[1601.01167](#)].
- [74] V. Shtabovenko, R. Mertig and F. Orellana, *FeynCalc 9.3: New features and improvements*, *Comput. Phys. Commun.* **256** (2020) 107478 [[2001.04407](#)].
- [75] Y. Aoki et al., *FLAG Review 2021*, [2111.09849](#).
- [76] J.L. Rosner, S. Stone and R.S. Van de Water, *Leptonic decays of charged pseudoscalar mesons*, *Review of Particle Physics 2021 update* (2021) .
- [77] C. Bourrely, I. Caprini and L. Lellouch, *Model-independent description of $B \rightarrow \pi \ell \nu$ decays and a determination of $|V_{ub}|$* , *Phys. Rev. D* **79** (2009) 013008 [[0807.2722](#)].
- [78] ETM collaboration, *Scalar and vector form factors of $D \rightarrow \pi(K) \ell \nu$ decays with $N_f = 2 + 1 + 1$ twisted fermions*, *Phys. Rev. D* **96** (2017) 054514 [[1706.03017](#)].
- [79] M.A. Ivanov, J.G. Körner, J.N. Pandya, P. Santorelli, N.R. Soni and C.-T. Tran, *Exclusive semileptonic decays of D and D_s mesons in the covariant confining quark model*, *Front. Phys. (Beijing)* **14** (2019) 64401 [[1904.07740](#)].

- [80] Y.-L. Wu, M. Zhong and Y.-B. Zuo, $B_{(s)}, D_{(s)} \rightarrow \pi, K, \eta, \rho, K^*, \omega, \phi$ Transition Form Factors and Decay Rates with Extraction of the CKM parameters $|V_{ub}|, |V_{cs}|, |V_{cd}|$, *Int. J. Mod. Phys. A* **21** (2006) 6125 [[hep-ph/0604007](#)].
- [81] A. Bharucha, D.M. Straub and R. Zwicky, $B \rightarrow V \ell^+ \ell^-$ in the Standard Model from light-cone sum rules, *JHEP* **08** (2016) 098 [[1503.05534](#)].